Uptake and reversibility of aluminium in calcium silicate hydrates

Master Thesis
by
Inga Mathilde Tangen

Aalborg University
Department of Chemistry and Bioscience
Fredrik Bajers Vej 7H
DK-9220 Aalborg

AALBORG UNIVERSITY
STUDENT REPORT

Department of Chemistry and Bioscience
Fredrik Bajers Vej 7H
9220 Aalborg Ø
http://www.bio.aau.dk

Title:
Uptake and reversibility of aluminium in calcium silicate hydrates

Theme:
Cement Chemistry

Semester: Master thesis

Timeframe: 01.09.20 - 06.08.21

ECTS: 60

Supervisors:
Yuanzheng Yue
Barbara Lothenbach
Yiru Yan

Number of pages: 80
Number of appendices: 4 (A-D)

Abstract

Production of Portland cement (PC) is responsible for a significant amount of anthropogenic CO_2 emissions, and ways to lower emissions are highly sought after. One way of reducing emissions is by substituting part of the cement clinker with supplementary cementitious materials (SCMs). SCMs typically contain more silica and alumina and less calcium than ordinary PC, which could change the compositoin of hydrated cement and C-S-H. This study aims to determine how the kinetics and reversibility of aluminium uptake in calcium silicate hydrates (C-S-H) changes, based on its composition. Specifically, it investigates how the Ca/Si molar ratio of C-S-H changes the kinetics of aluminium uptake and properties of the resulting solids, as well as whether the aluminium uptake is reversible.

In order to investigate the kinetics of aluminium uptake, 240 samples of varying Ca/Si and Al/Si molar ratio with varying hydration time were synthesised and analysed. The results showed slower uptake of aluminium in low Ca/Si samples, compared to high Ca/Si. Additionally, the inclusion of aluminium increases the mean chain length (MCL) of the C-S-H by binding to bridging tetrahedra in C-S-H. In target Ca/Si ≤ 1.0 and Al/Si ≤ 0.05, all the Al goes to C-S-H.

Furthermore, the reversibility of the aluminium uptake in C-S-H was tested by synthesising samples of calcium aluminium silicate hydrate (C-A-S-H) that were filtered and added to a solution without aluminium. The results showed that aluminium is reversible in low Ca/Si C-S-H short-term, with an increasing stability of Al in C-S-H with higher Ca/Si.

These results suggest that PC which is partially substituted by SCMs will have increased MCL due to the incorporation of more aluminium. As PC systems are complex, the reversibility of aluminium uptake in C-S-H does not necessarily mean that aluminium will be equally reversible in PC systems.

Dansk Resume

Produktion af Portland Cement (PC) er ansvarligt for en stor del af den menneskeskabte udledning af CO_2, derfor er muligheder for at sænke udledningen, eftersøgt i stor stil. En af måderne udledning kan reduceres på, er at substituere dele af cementklinkeren med såkaldte "supplementary cementitious materials" (SCM). SCM indeholder generelt mere silica og aluminiumoxid, og mindre calcium end regulært PC. Dette studie forsøger at fastlægge, hvordan kinetikken og reversibiliteten af aluminium i calcium silikat hydrat (C-S-H) ændres, baseret på dennes sammensætning. Specifikt, så undersøger den hvordan Ca/Si molar forholdet af C-S-H ændrer kinetikken af aluminium optag og egenskaberne af det resulterende materiale, og om aluminium optaget er reversibelt.

For at undersøge kinetikken af aluminium optag, skulle 240 prøver af forskellige Ca/Si og Al/Si molar forhold, med varierende hydrationstider, syntetiseres og analyseres. Resultaterne viste langsommere optag af aluminium i lav Ca/Si prøver, i forhold til høj Ca/Si, hvilket indikerer at den delvise subsituering af PC klinker med SCM vil retardere optaget af aluminium i C-S-H'et af cement. Derudover øger inkluderingen af aluminium den gennemsnitlige kædelængde (MCL) af C-S-H'et ved at binde brobyggende tetraedre i C-S-H. I Ca/Si ≤ 1.0 og Al/Si ≤ 0.05, bliver alt aluminium optaget i C-S-H.

Reversibiliteten af aluminium i C-S-H'et blev testet, ved at syntetisere prøver af calcium aluminium silikat hydrat (C-A-S-H) som blev filtreret og tilføjet til en opløsning uden aluminium. Resultaterne viser at aluminium er reversibelt i lav Ca/Si C-S-H, med en øgende stabilitet af Al for højere Ca/Si C-S-H.

Disse resultater antyder at PC, som er delvist substitureret af SCM, vil have højere niveauer af MCL, på grund af inkluderingen af mere aluminium. Da PC systemer er komplekse, betyder det ikke nødvendigvis at aluminium vil være reversible i PC systemer, selvom det måske er muligt i lav Ca/Si C-S-H.

Preface

This report was completed during the period of September 1st 2020 to August 6th 2021 as a Master thesis project in chemistry at Aalborg University, under guidance of Yiru Yan, Barbara Lothenbach, and Yuanzheng Yue. The purpose of this master thesis was to examine the kinetics and reversibility of aluminium uptake in the C-S-H phase of cement.

Thank you to my supervisors Barbara, Yiru and Yuanzheng the opportunity to work on this project, and for your guidance and discussions throughout the project. A special thank you to Yiru. I truly appreciate your help and feedback during the project, and for teaching me on the world of C-S-H. I also want to thank Zhencai Li for your invaluable help in the lab, even during vacations, weekends and evenings.

Additionally, I would like to thank the following people, who all played a part in helping me with the project:

- Bin Ma (Empa, co-supervisor)
- Lab technicians Henriette C. Jensen and Anne Flensborg
- Jørgen Skibsted (AU, solid-state NMR analysis)
- Fred Sheng-Yu Yang (AU, solid-state NMR analysis)
- Benedicte Snedker Halvorsen (XRD sample preparation)
- Rasmus Skov Klitgaard Madsen (XRD supervision)
- George-Dan Miron (PSI, GEM-Selektor model for C-A-S-H system)
- Søren Strandskov Sørensen (TGA supervision)
- Katharina Xenia Kaiser (TGA supervision)

When reading this report, a fundamental understanding of chemistry is expected. The abbreviations used in the report appear in the abbreviation list. Citations are stated with numbers, [number], with a corresponding number in the bibliography. The references in the report are listed according to the Harvard citation method, and the information on the references can be found in the bibliography. When the reference is at the end of a paragraph, the entire paragraph is based on the reference. Otherwise the reference can be found after the theorem. Figures and tables without references are made by the author. The appendix includes supplementary information such as tables containing weigh-in masses and TGA results, concentrations of elements measured by ICP-OES, and mass balances. A .zip file containing data from XRD, TGA, ICP-OES and pH is available.

List of Abbreviations

Abbreviation	**Meaning**
BFS	Blast furnace slag
C-A-S-H	Calcium aluminium silicate hydrate
CCN	Cement chemist notation
CH	Portlandite
C-S-H	Calcium silicate hydrate
FA	Fly ash
FT-IR	Fourier-transform infrared spectroscopy
Hc	Hemicarbonate
ICP-OES	Inductively coupled plasma optical emission spectrometr
MAS	Magic angle spinning
Mc	Monocarbonate
NMR	Nuclear magnetic resonance
OPC	Ordinary Portland cement
PC	Portland cement
SCM	Supplementary cementitious materials
TAH	Third aluminate hydrate
TGA	Thermogravimetric analysis
XRD	X-ray diffraction

Contents

Introduction 1

Portland cement (PC) production has increased steadily for the past 100 years, with a current production of more than 4 billion tonnes annually, making it the second most consumed material after water. [1, 2] The increase in production expects to continue, as PC has an essential role in buildings and infrastructure worldwide. As PC production accounts for up to 8 % of the global carbon dioxide emission, there is a need to lower the carbon footprint associated with it. The CO_2 emission is partly the result of limestone ($CaCO_3$) calcination. Decomposition of limestone is inevitable when producing PC clinker and results in approximately 0.5 tonne CO_2 per tonne of clinker produced. [2] In addition, the rotating kiln furnace in PC production is heated to approximately 1450 °C, which contributes further to the emission. [3]

Supplementary cementitious materials (SCMs), such as blast furnace slags, byproducts from steel production, fly ash, or calcined clays, require less energy than PC to produce, and can be implemented as a partial substituent for PC in order to lower the carbon footprint of PC production. [2, 4] The use of SCMs can enhance desirable properties of cement, including the strength and durability. [5] It has been found that SCMs can increase the compressive strength by 20 % compared to that of ordinary PC (OPC), while simultaneously reducing the CO_2 emission by up to 20 %. [3] In addition, the use of SCMs can help with the recycling of waste products from other industrial processes, which otherwise contribute to pollution when dumped in open landfills. [5] While OPC has a Ca/Si molar ratio between 1.5 - 1.9, SCM blends can have significantly lower ratios of between 0.6 - 1.9. Variation of the Ca/Si molar ratio affects the calcium silicate hydrate (C-S-H) phase of cement, and subsequently, the properties of the cement. [2]

Byproducts such as blast furnace slag and fly ash are typical SCMs that contain a higher amount of aluminium than in OPC, leading to the incorporation of more aluminium in the C-S-H phase. [6] Aluminium can substitute for the silica present in C-S-H and can thus change the structure of C-S-H. [7] The introduction of aluminium to the C-S-H phase might change the cohesion and durability of the material. Thus it is important to gain more knowledge on the structural and kinetic properties of the C-A-S-H phase. [6] Furthermore, it is imperative to understand the reversibility of aluminium uptake in C-S-H with varying Ca/Si molar ratio, to determine the stability of C-(A)-S-H phases. A better understanding of Al sorption in C-S-H is needed to improve on existing thermodynamic models of C-S-H, which can help engineer cement for the future. [2,8]

In order to investigate the kinetics of aluminium uptake in systems resembling SCM blends, C-S-H with a target molar ratio of between 0.6 and 1.6 were synthesised. A target Al/Si molar ratio of between 0.0003 and 0.1 was prepared for each of the different Ca/Si molar ratios, and all samples were analysed at different hydration times. A reversibility experiment was performed in order to determine the relative stability of the aluminium uptake in the C-S-H phase.

1.1 Problem Statement

More data is needed on the kinetics of aluminium uptake in calcium silicate hydrates (C-S-H), particularly to improve thermodynamic modelling of more sustainable cement. In order to obtain this data, an extensive data set of various calcium/silicon and aluminium/silicon molar ratios will be investigated in this project. The effect of hydration time on the ratio of different Al sites in C-S-H will be studied. Additionally, there is limited knowledge on the reversibility of aluminium uptake in C-S-H, which is valuable knowledge when it comes to degradation of partially substituted PC. The reversibility of aluminium in various calcium/silicon C-S-H will thus also be investigated.

How does the composition of the C-S-H phase influence the uptake and reversibility of aluminium into the C(-A)-S-H phase, and what do the obtained results indicate for durability of blended Portland cement systems that are partially substituted by supplementary cementitious materials?

Theory 2

2.1 Cement

In order to understand the role of aluminium in C-S-H, it is necessary to have some knowledge of the composition and chemistry of cement. Cement is a hydraulic binder, which means that it reacts with water to form an adhesive material. The processes that lead to the hardening of the cement are called hydration reactions. After the cement has hardened, it can retain its strength and stability in most natural environments, even underwater. [9]

Portland cement (PC) is produced in three main steps: First, raw materials like clay, shale, sand, and limestone are gathered and mixed. Then, the raw materials are heated in a rotating kiln in order to produce cement clinker. Finally, the clinker is ground to a powder and gypsum ($CaSO_4$) is commonly added to avoid hydration to start too rapidly [10,11]. Figure 2.1 shows the change from raw materials to clinker as the temperature increases in the kiln. In order to achieve high early strength, alite is desired [10]. Additionally, the cement clinker should be produced at a reasonable rate, which requires partial melting of the clinker. Thus, the rotating kiln furnace temperature commonly reaches a temperature of at least 1450 °C [3,10].

A notable amount of the global CO_2 emission comes from cement production. Calcining of limestone releases a significant amount of CO_2, as shown in Figure 2.1 and in Equation 2.1. Additionally, a high amount of energy and fuel is required for clinker production, in order to reach the high temperature necessary. As the global demand for cement is increasing, there is a need for ways to lower the emissions as much as possible. Through improved technology and better processing, energy efficiency has been improved. The use of alternative fuels has been implemented as another way to lower emissions. In addition, SCM are commonly used as clinker substitutes to recycle waste from power production and lower the energy needed for cement production. [12]

$$\mathrm{CaCO_3}(s) \longrightarrow \mathrm{CaO}(s) + \mathrm{CO_2}(g) \tag{2.1}$$

PC is the type of cement most commonly used. The clinker used in PC consists mainly of silica (SiO_2) and calcium oxide (CaO). There are often minor contents of alumina (Al_2O_3) and ferrite (Fe_2O_3) as well. Hydraulic hardening of cement is

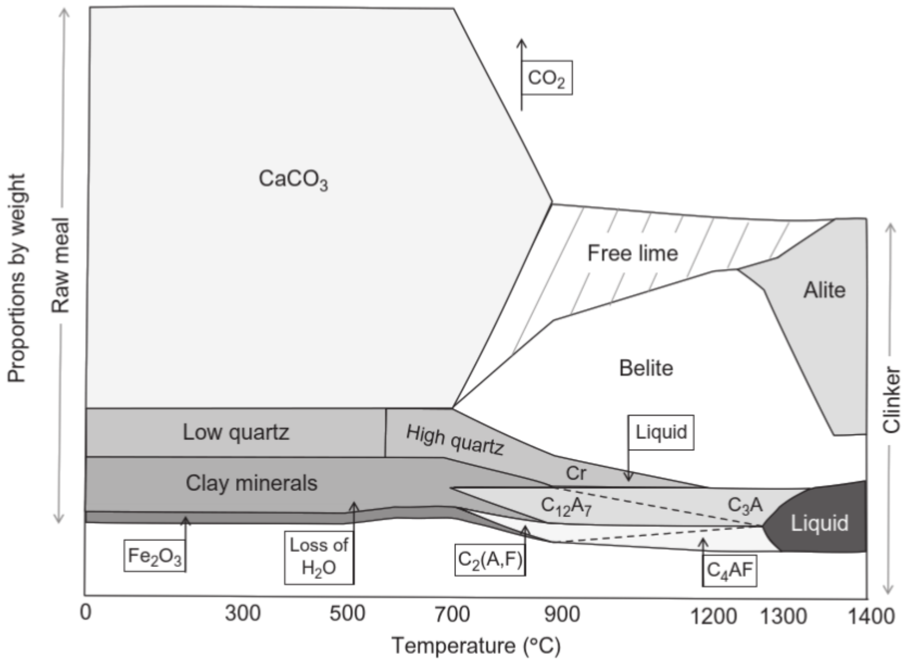

Figure 2.1: Proportions of materials present during conversion from raw material to clinker, as temperature increases. [9]

primarily due to the hydration of calcium silicates, but chemical compounds such as aluminate might also participate in the hardening process. [9]

The components of cement are often denoted by their cement chemist notation (CCN), in order to shorten the chemical formula. The CCN, IUPAC name, chemical formula and phase name of the most common clinker phases are listed in Table 2.1. The individual phases are discussed in detail in Section 2.2.

Table 2.1: CCN, chemical formula, IUPAC name and phase name for the four most common crystalline phases of cement clinker.

CCN	Chemical formula	IUPAC name	Phase name
C_3S	$3\,CaO \cdot SiO_2$	Tricalcium silicate	Alite
C_2S	$2\,CaO \cdot SiO_2$	Dicalcium silicate	Belite
C_3A	$3\,CaO \cdot Al_2O_3$	Monocalcium aluminate	Aluminate
C_4AF	$4\,CaO \cdot Al_2O_3 \cdot Fe_2O_3$	Calcium aluminoferrite	Ferrite

2.2 Cement hydration

Hydration can be defined as the reaction of an anhydrous compound with water, creating a new compound, namely a hydrate. When it comes to cement, hydration is defined as the reaction of a non-hydrated cement or one of its constituents with water. This brings about chemical and physico-mechanical changes of the system, particularly in regards to setting and hardening of the cement paste. For a complete hydration to occur, the cement must be mixed with sufficient amounts of water. The water/cement ratio affects the properties of the hydrated material. Normally, water/cement ratios of around 0.3 to 0.6 have paste consistency and is called fresh cement paste. These types of pastes set and harden during the hydration process and are converted to a hardened cement. When the cement paste is setting, it loses its plasticity in a sudden fashion and is converted into a solid material. When the cement is hardening, there is a development of hardness and strength that follows the setting of the paste. [9]

Portland cement (PC) is a multi-component system, and its hydration process is rather complex, where a series of individual chemical reactions take place both successively and at the same time. Heat is liberated during the process, as it is an exothermic event. Factors such as the phase composition of the cement, the fineness of the particles, curing temperature, ratio of water to cement, and presence of chemical admixtures, can influence the hydration and its kinetics. [9]

The hydration of PC can be divided into the pre-induction, the induction, the acceleration, and the post-acceleration period. During the initial minutes of hydration, the pre-induction period takes place. The first hydration products are formed as the surface of the clinker minerals are partially dissolved upon wetting. The induction period continues for the first 1-2 hours of hydration. It is primarily alite that is reacting. At this point, the clinker is covered by a layer of hydration products, which leads to a reduced hydration rate. The acceleration period takes place 3-12 hours into hydration, and leads to nucleation and growth of hydration products. Finally, the post-acceleration period starts, in which the hydration continues based on diffusion of solids. During this period, belite hydration increases and alite hydration decreases. [11]

There are four main hydration phases of PC, namely alite, belite, aluminate, and ferrite. Figure 2.2 shows the formation of the hydrates as a function of time. Hydration starts immediately upon contact with water, when the pre-induction period happens. After a few minutes, the induction period starts, and the reaction rate slows down significantly. The hydration accelerates after a few hours, in what is called the acceleration period, and reaches its maximum after approximately 5-10 hours. Then, the hydration rate slows down gradually during the deceleration period. However, there may be a measurable hydration even after months of curing. When the non-reacted alite is consumed, the reaction slows down, and finally stops altogether. [9]

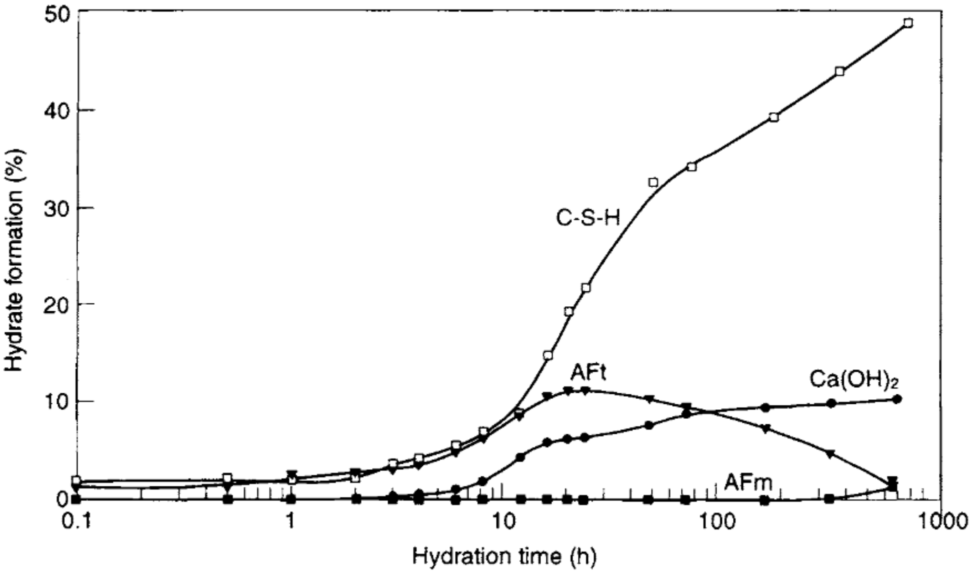

Figure 2.2: Formation of hydrates plotted against time. [9]

Alite ($3\,CaO \cdot SiO_2$,C_3S) is the main hydration product of PC, and is responsible for the early strength of hydrated cement.The C_3S present in PC is called alite. It is impure due to doping with other ions that are present in the PC clinker. The exact composition and reactivity of alite varies in different cements, and its hydration is complex and not fully understood. [9]

The hydration of alite is followed by the formation of calcium hydroxide ($Ca(OH)_2$, CH), also called Portlandite, as shown in Equation 2.2. In hydration of C_3S, most of the calcium hydroxide precipitates as solid CH crystals. CH becomes evenly distributed throughout the formed cement paste. Although there has been previous discussion on whether CH can be amorphous, there has been no convincing data on this. CH has a hexagonal structure consisting of calcium ion layers that are octahedrally coordinated, and CH coordinated oxygen layers, where hydrogen is bound to the oxygen. [9]

$$2\,C_3S + 7\,H \longrightarrow C_{1.5}{-}S{-}H_2 + 3\,CH \tag{2.2}$$

Belite ($2\,CaO \cdot SiO_2$, C_2S) is the second most abundant phase in cement clinker, and its hydration reaction is shown in Equation 2.3. Belite is less reactive than alite at early ages, but can contribute significantly to the strength of cement at later ages. The production of belite requires less CaO than for alite, and thus also a lower CO_2 emission. However, because of the delayed reactivity, alite cements are more utilised. Additionally, alite cements react better with SCMs, and can thus help reduce CO_2 emissions that way. [9]

$$2\,C_2S + 4\,H \longrightarrow 2\,C_{1.5}{-}S{-}H_{1.5} + CH \tag{2.3}$$

Aluminate ($3\,CaO \cdot Al_2O_3$, C_3A) is the most reactive PC clinker phase. In the presence of water, hydroxy-AFm is produced. The hydration is shown in Equation (2.4). Aluminate will flash set within minutes without the addition of gypsum ($CaSO_4 \cdot 2\,H_2O$). When aluminate is in the presence of gypsum during hydration, ettringite is formed instead of hydroxy-AFm, as shown in Equation (2.5). [13]

$$C_3A + CH + 12\,H \longrightarrow C_4AH_{13}\ \text{(Hydroxy-AFm)} \tag{2.4}$$

$$C_3A + 3CSH_2 + 26H \longrightarrow C_3A - 3CS - 32H\ \text{(Ettringite, AFt)} \tag{2.5}$$

Ferrite ($4\,CaO \cdot Al_2O_3 \cdot Fe_2O_3$, C_4AF) reacts similarly to aluminate during early hydration, although with a slower hydration reaction. Like aluminate, ferrite forms ettringite, CH and alumino hydroxide during hydration, as shown in as shown in Equation (2.6). Ferrite reacts further with ettringite, which produces monosulphate, as shown in Equation (2.7). Monosulphate does not contribute to the compressive strength of the cement [11].

$$C_4AF + 3CSH_2 + 3OH \longrightarrow C_6AS_3H_{32} + CH + FH_3 \tag{2.6}$$

$$2C_4AF + C_6AS_3H_{32} + 12H \longrightarrow 3C_4ASH_{12} + 2CH + 2FH_3 \tag{2.7}$$

2.3 Supplementary cementitious materials

A high consumption of natural, non-renewable resources is seen in the cement industry. With the increasing demand for cement, the need for raw materials will be difficult to sustain long term. Large amounts of waste materials are generated from several sources, including manufacturing processes, industries and municipal solid waste. These waste materials pose a problem when it comes to recycling, and will often end up in landfills. The waste products can be utilised as supplementary cementitious materials (SCMs) to partially replace Portland cement (PC) clinker, which can reduce the problem with waste recycling and simultaneously help with the growing demand for cement. [14]

The most commonly used SCM is fly ash (FA), which is a by-product from combustion of coal in thermal power plants. FA mainly consists of silica, alumina, and calcium, and can display pozzolanic reactivity [14]. Pozzolans do not possess much cementitious value by itself, but if ground finely and in the presence of $Ca(OH)_2$ or in aqueous alkaline conditions, the pozzolan can display pozzolanic reactivity [15]. Pozzolanic reactivity means that the pozzolan can form hydration products similar to those of PC [3].

Other common SCMs are blast furnace slag (BFS) from pig iron production, pozzolanic clay minerals such as metakaolin (MK) and ash from incineration of e.g. municipal solid waste and other industrial processes [14]. Table 2.2 shows the composition of PC and FA. FA generally contains more SiO_2, Fe_2O_3, and Al_2O_3 than PC. Other SCMs, such as BFS, also contain significant amounts of Al, which is released into solution and can affect the properties of the C-S-H and cementitious system. Due to the increased content of Al_2O_3 in common SCMs, it is of interest to gather more data on the kinetics of Al uptake in C-S-H, as this can influence the setting and properties of the cement blend.

Table 2.2: Common composition of PC and range of elements in FA in %.

Component	**Average PC (%) [9]**	**Range FA (%) [14]**
SiO_2	21.02	11.8 - 62.8
Fe_2O_3	2.85	1.4 - 24.4
Al_2O_3	5.04	2.6 - 35.6
CaO	64.18	0.5 - 54.8
MgO	1.67	0.1 - 6.7
SO_3	2.58	0.0 - 12.9
Na_2O	0.24	0.1 - 3.6
K_2O	0.70	0.1 - 9.3
Other	1.72	-

Figure 2.3 shows the reactivity of FA, BFS, and MK compared to alite, for clinker replacements of between 30 and 50 wt%. The reaction degrees of these SCMs

are significantly lower and slower than for alite. The slower reaction degree leads to a decrease in early strength when SCMs are partially substituting PC clinker. However, the reaction degree varies with different SCMs, and it is thus possible to design the cementitious system based on the prefered properties of the cement. For instance, metakaolin can reach up to 100% degree of reaction with prolonged hydration, when up to 20 wt% clinker is substituted by it. Most SCMs contribute to long-term strength development, as their reaction is quite slow compared to alite. With long-term hydration, it is possible that SCMs might lead to comparable or exceed the strength of OPC. Additionally, the long-term durability might be enhanced, while simultaneously improving the sustainability of cement production. [15]

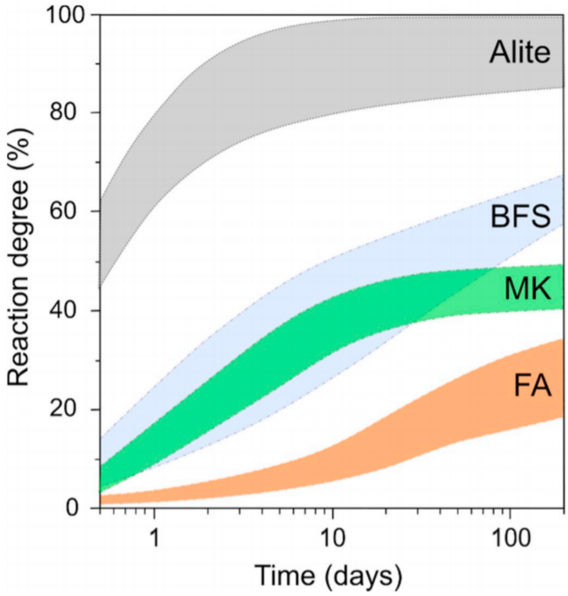

Figure 2.3: Reactivity of common SCMs compared to alite. FA: Fly ash, BFS: Blast furnace slag, MK: Metakaolin. Figure from [15].

The reactive components in SCMs are often amorphous or glassy phases, and their reactivity is largely influenced by their chemical composition and structure. The main reactive phases of FA and slags are aluminosilicate and calcium aluminosilicate glasses, respectively. Minor elements such as magnesium, sodium, potassium and iron are also incorporated as oxides. The amorphous phase generally consists of silicate (SiO_4) and aluminate (AlO_4) tetrahedra bound together in a polymerised network by bridging oxygens (BOs), as depicted in Figure 2.4. Cations such as Ca^{2+} and Na^+ act as either charge balancing ions or as network-modifying cations. Network modifiers distort the silicate or aluminosilicate network, forming non-bridging oxygens (NBOs) that are linked to the network modifier. This in turn leads to a lower degree of polymerisation, which is commonly expressed at Q^n, where n = 0, 1, 2, 3, or 4. The more connected the network is, by BOs, the more polymerised the system is. For instance, a Q^0 indicates that the SiO_4 or AlO_4 tetrahedra are not connected to any other tetrahedra, while a Q^4 means that all the oxygens on the tetrahedra are connected to other tetrahedra. Lower degrees of polymerisation often lead to higher reactivity. [15]

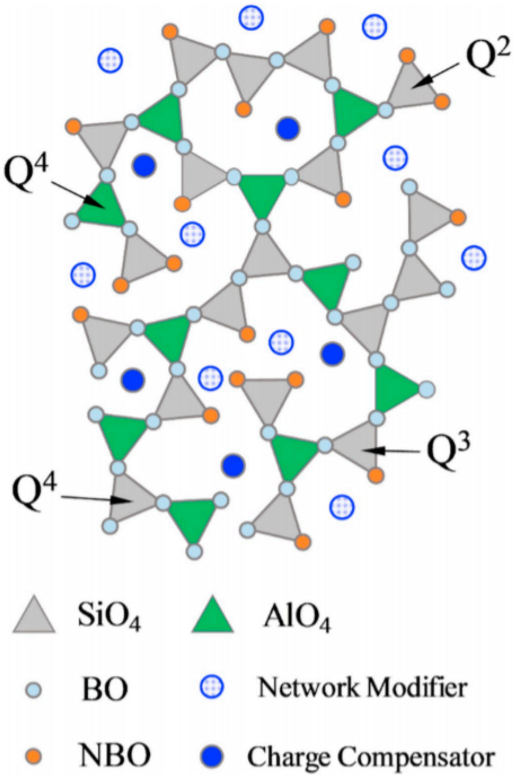

Figure 2.4: Illustration of the disordered structure of an aluminosilicate glass. Figure from [15].

In this project, C-S-H and C-A-S-H of varying Ca/Si are synthesised. Although they are not of amorphous nature, the polymerisation plays an important role in understanding their properties and how they change with varying Ca/Si and Al/Si molar ratios.

2.4 Calcium silicate hydrate

When C_2S and C_3S react with water, C-S-H is produced. C-S-H is sometimes described as a poorly crystalline gel rather than a crystalline material, as no consistent structure can be discerned by X-ray diffraction alone [9, 16]. However, electron microscopy has revealed a crystalline character to C-S-H [17]. Thus, it is likely more correct to describe C-S-H as a nano crystalline material, where the Ca/Si molar ratio of the C-S-H can vary widely within each sample. C-S-H is the main component in hydrated cement and is responsible the cohesive properties of the cement paste [6]. Equation 2.8 and 2.9 show the formation of C-S-H from the hydration of C_3S and C_2S, respectively.

$$3\,\mathrm{CaO}\cdot\mathrm{SiO_2} + (3+m-n)\mathrm{H_2O} \longrightarrow \mathrm{nCaO}\cdot\mathrm{SiO_2}\cdot\mathrm{mH_2O} + \text{(3-n)}\mathrm{Ca(OH)_2} \qquad (2.8)$$

$$2\,\mathrm{CaO}\cdot\mathrm{SiO_2} + (2+m-n)\mathrm{H_2O} \longrightarrow \mathrm{nCaO}\cdot\mathrm{SiO_2}\cdot\mathrm{mH_2O} + \text{(2-n)}\mathrm{Ca(OH)_2} \qquad (2.9)$$

While the structure of C-S-H is still debated, it is generally believed to have a layered structure similar to that of the mineral tobermorite [6], as can be seen in Figure 2.5. There are three different types of tobermorite, namely 9Å, 11Å, and 14Å. They have different basal spacing and water content. Tobermorite 11Å is the most widely used model for C-S-H characterisation [16].

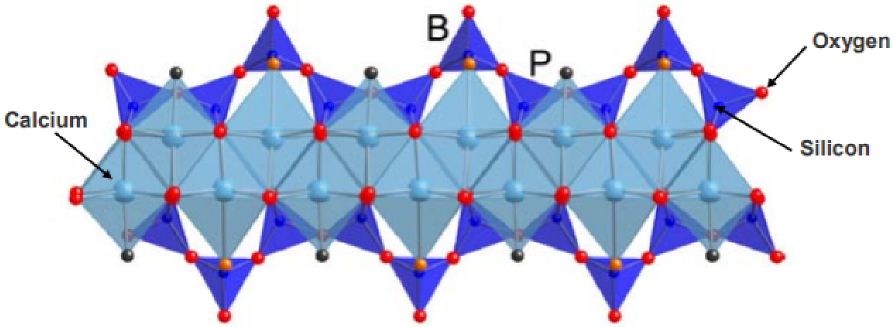

Figure 2.5: Illustration of an idealised tobermorite structure. Figure from [18], modified from [19].

Both C-S-H and tobermorite have a calcium layer with linear silicate chains on each side of the plane, arranged in a "dreierketten" structure, which is a repeating chain of three silica tetrahedra. The silicate tetrahedra linked to the calcium oxide layer are named pairing tetrahedra, while the bridging tetrahedron links the two pairing tetrahedra [16].

Tobermorite has a Ca/Si molar ratio close to 0.7, which corresponds to infinite silicate chains [6]. The stoichiometry of C-S-H varies, where the Ca/Si ratio is usually between 0.6 and 1.9 [2]. In PC, Ca/Si molar ratios range between 1.5 to 1.9, while SCM blends typically contain lower Ca/Si ratios. In PC, there is a high initial calcium concentration stemming from the dissolving of alite, and the pore solution is supersaturated with respect to CH. The activity of calcium hydroxide is higher than for synthetic C-S-H, which leads to precipitation of C-S-H richer in calcium in PC than in synthetic C-S-H. The mean chain length for C-S-H in PC is close to 2, indicating that most of the bridging tetrahedra have disappeared, and that mostly dimers are present. [7]. Figure 2.6 and Figure 2.7 show the relation between solid Ca/Si ratio of synthetic C-S-H and aqueous concentration of calcium and silicon, respectively, in solution absent of aluminium or alkalis.

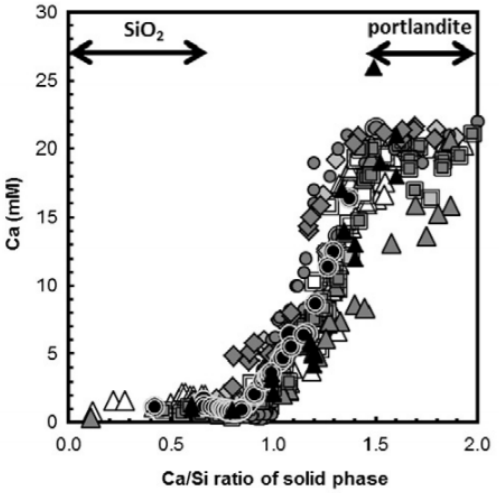

Figure 2.6: Ca/Si in solids against aqueous concentration of Ca. [7]

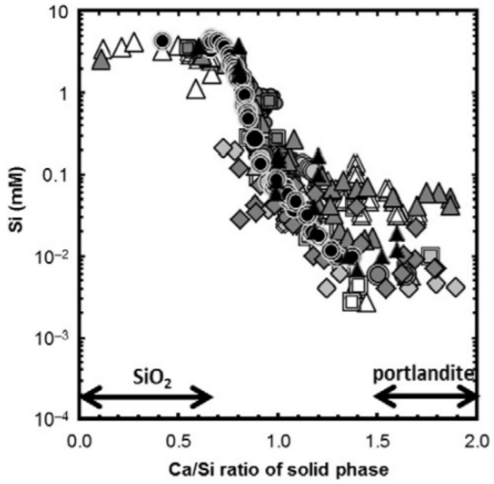

Figure 2.7: Ca/Si in solids against aqueous concentration of Si. [7]

The mean chain length (MCL) of silica varies with Ca/Si ratio, where an increase in Ca/Si leads to a shorter MCL. Ca/Si = 1.0 typically have MCL of 7 or higher, while pentamers are dominant in Ca/Si $\approx$ 1.2. At higher Ca/Si, dimers are prevalent [16].The Ca/Si molar ratio can influence the compressive strength of the cement, where it has been found that decreasing Ca/Si C-S-H have increasing compressive strength, compared to higher Ca/Si C-S-H, as shown in Figure 2.8. [20] It is possible that the increased compressive strength is caused by the increased MCL in low Ca/Si, although it is not known for certain if it is the main contributor to the change. For instance, there is a difference in specific surface area of the C-S-H, depending on the Ca/Si molar ratio. Even though there are smaller cohesive forces in low Ca/Si ratio C-S-H, the specific surface area might compensate and increase the compressive strength overall [20].

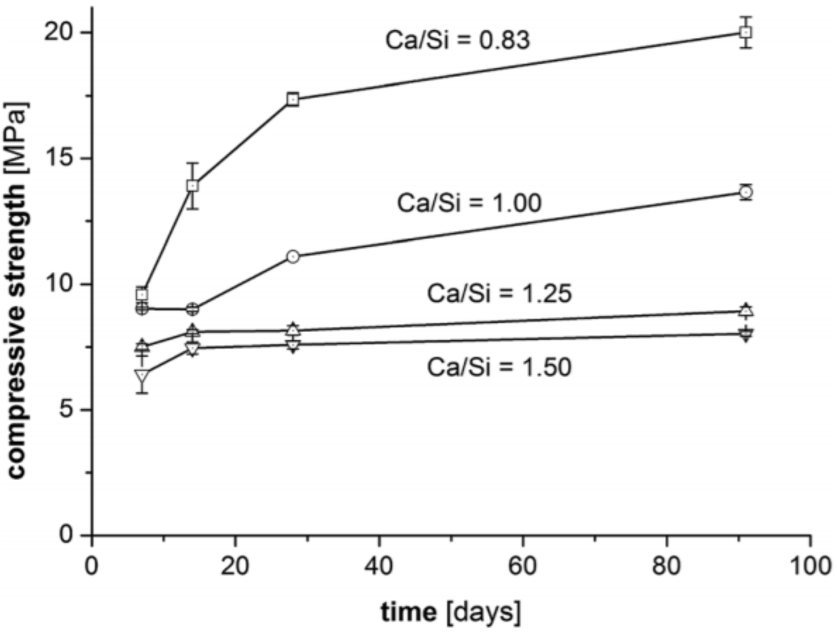

Figure 2.8: Development of compressive strength for C-S-H with varying Ca/Si molar ratio. [20]

The surface of C-S-H is charged, due to deprotonation of silanols with increased pH, in addition to interaction with calcium [21]. It is important to model the charge of the surfaces, as it plays an important role in material cohesion and in interaction with admixtures [21]. Alkali ions compete with calcium ions to compensate the negative surface charge. Bivalent cations such as calcium are strongly favoured compared to monovalent cations such as sodium and potassium, due to their stronger electrostatic interaction. Thus, high calcium concentrations can inhibit alkali uptake. In other words, high Ca/Si C-S-H has a low alkali uptake compared to low Ca/Si C-S-H [7].

Even though C-S-H is not crystalline, some diffraction peaks can be observed. As the Ca/Si ratio increases, the peak at $\approx 7\ ^\circ\ 2\theta$ and d-value of 1.26 nm shifts to higher values, which indicates a decrease of the basal spacing [16]. Increased Ca/Si ratios also lead to a higher water content, which is correlated to the increased basal spacing, and higher density [7].

2.5 Calcium aluminium silicate hydrate

C-S-H incorporates aluminium readily, which leads to the formation of C-A-S-H at Al/Si ≤ 0.1. At higher Al/Si ratios, aluminium is taken up in katoite (C_3AH_6) and/or strätlingite (C_2ASH_8), in addition to C-A-S-H [22]. In the silica dreierketten structure, aluminium is mainly taken up in the bridging position, which leads to an increased chain length [23]. Furthermore, the aluminium uptake in C-S-H increases as the concentration of aluminium in the aqueous phase increases. At higher pH, strätlingite is destabilised, which increases the dissolved aluminium concentration and in turn leads to higher aluminium uptake in C-S-H [22].

In the early age of hydration, the cohesion of cement paste is caused by attractive electrostatic forces between charged C-S-H particles. When Al^{3+} is introduced, it substitutes for some of the Si^{4+} in C-S-H, which introduces a negative permanent charge. This charge can influence the cohesion forces. [6]

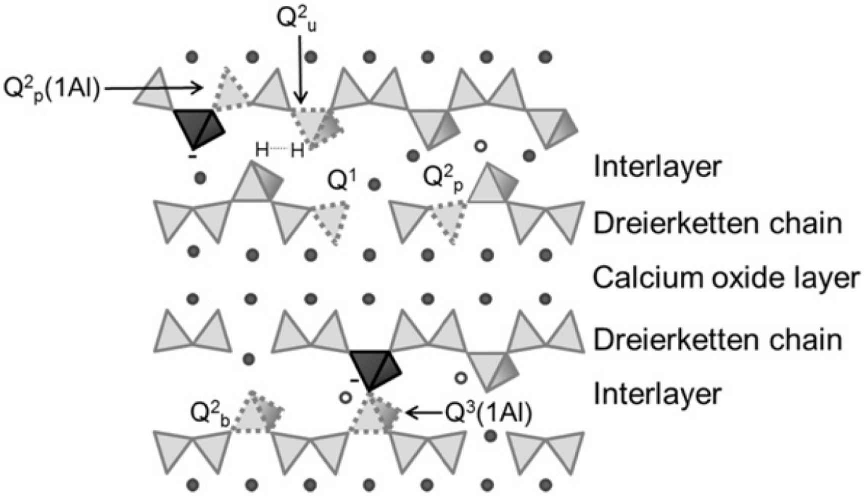

Figure 2.9: Schematic of C-A-S-H. [22] Ca is shown as grey circles in the interlayer between the silica chains. The clear circles represent water or alkali species. The light grey tetrahedra are SiO_4^-, while the dark grey tetrahedra are AlO_4^-. [22]

Figure 2.9 shows a schematic of C-A-S-H. In the $Q^n_{(mAl)}$ notation for polymerisation, n indicates the numbers of silicon neighbours and m the number of aluminium neighbours. A 'b' or 'p' subscript denotes a bridging or pairing position, respectively. The substitution of aluminium occurs primarily as tetrahedrally coordinated Al^{IV} in the bridging position (Q^2_b). Aluminium has also been reported in Q^3 sites that link two dreierketten chains together in tobermorite. [22]

With an increase in Ca/Si molar ratio, the relative amount of Al^{IV} decreases, and a higher amount of octahedrally coordinated Al^{VI} is observed, as shown in Figure 2.10. Previous studies suggest that Al^{VI} corresponds to either an amorphous aluminium hydroxide or calcium aluminate hydrate at the C-S-H surface, or to a calcium aluminate hydrate in the interlayer of the C-S-H [16]. Approximately 10% of the aluminium present in C-S-H is pentacoordinated (Al^{V}), regardless of the Ca/Si ratio [22]. A higher uptake of aluminium has been observed in C-S-H with higher Ca/Si ratios. This could be caused by the calcium stabilising the interlayer on aluminium uptake [2].

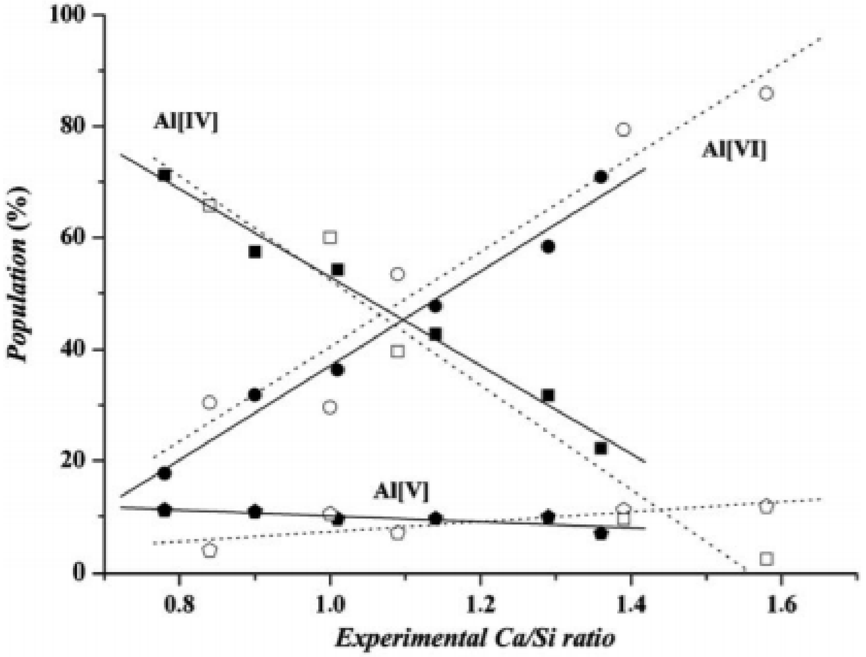

Figure 2.10: Population change of environment for aluminium in C-S-H with varying Ca/Si. [24]

Increased pH values lead to higher dissolved aluminium concentrations and ensures that precipitation of secondary phases, such as aluminium hydroxide, is avoided. [2] Thus, a higher pH in solution can ensure that more aluminium is incorporated into the C-S-H. The amount of aluminium incorporated in C-S-H increases with decreasing Ca/Si ratio and with increased dissolved aluminium concentration in solution. NMR studies indicate that the aluminium uptake in synthetic C-S-H increases in the presence of alkali hydroxides. However, the distribution of aluminium species with varying coordination does not seem to be affected by alkali hydroxides. [16]

In low Ca/Si C-S-H, Al can substitute for Si. At Ca/Si $>$ 1, Al is bound in octahedral sites. Al can also be present in five-fold (Al(V)) and octahedral (Al(VI)) coordination. The five-fold coordinated Al is present in the interlayer of the C(-A)-S-H, and might be substituting some of the Ca^{2+} in the interlayer. [25] In high Ca/Si, it is believed that Al is in the interlayer of the C(-A)-S-H, increasing the basal spacing. [25] Al(VI) is also believed to be bound in an amorphous hydrate associated with C-A-S-H precipitation, called third aluminate hydrate (TAH). TAH "could correspond to the intercalation of a single layer of AFm between precipitating C-S-

H or to a separate phase at the surface of C-S-H" [7]. However, recent studies debate that TAH does not exist, and that Al in high Ca/Si is stabilised by hydroxyl groups when these are present [26]. Although TAH is debated, it is the most acknowledged theory on Al in high Ca/Si, to the best of the authors knowledge.

Several studies have focused on the effects of Al uptake on the C-S-H structure. However, there is limited data on the effect of time when it comes to Al uptake C-S-H. Furthermore, the reversibility of Al in C-S-H has not been researched extensively. Research on this can help develop thermodynamic model databases that can help predict the kinetics and reversibility of Al uptake in C-S-H, and furthermore, to model SCM systems for practical use.

2.6 Considerations for experiment

The experimental procedure was developed based on several previous studies [2, 16, 22, 27], and modified according to the available equipment in the laboratory. The goal was to synthesise C-S-H, and C-A-S-H, in a simple way and without too many variables.

The simplest way to synthesise C-S-H is to mix the raw materials of CaO and SiO_2 at room temperature, together with water. An aqueous solution can also be used, but the ions present should be considered carefully, as they might change the chemistry of the C-S-H. For this project, an aqueous solution of NaOH was chosen, because it is alkaline like the pore solution in Portland cement (PC) [7, 16], and can thus help model a more realistic cementitious system. Additionally, high pH might help promote hydrolysis of silicates in solution, which starts the C-S-H formation [28]. SiO_2 fume was chosen instead of SiO_2 with bigger particle size, in order to increase the kinetics of C-S-H formation.

Experimental methods 3

The weigh-in masses of the samples are shown in Appendix A, in Table A.2 and Table A.1, for the kinetics and reversibility synthesis, respectively. A description of the experimental method for the kinetics and reversibility synthesis, as well as for the analysis methods, are presented below.

3.1 Kinetics

The synthesis was performed in a two-step protocol, where C-S-H was firstly synthesised and equilibriated, before adding a source of aluminium, to obtain C-A-S-H. CaO was prepared by heating $CaCO_3$ for 12 hours at 1000 °C directly prior to use. Samples with a target Ca/Si molar ratio of 0.6, 0.8, 1.0, 1.2, 1.4, and 1.6 were synthesised by mixing of CaO and fumed SiO_2 powder with a 0.5M NaOH solution to obtain a W/S ratio of 45 (2 g solids, 90 mL solution). For each equilibration time, a separate sample was synthesised. The samples were made and stored in polyethylene containers with a lid and a volume of 100 mL. The samples were placed on a sample shaker with a speed of 175 mot/minute for 48 hours, and were subsequently shaken by hand daily until filtration. To each sample, a $NaAlO_2$ solution of 5, 10, 50, or 100 mmol/L was added after 14 days of mixing, in order to obtain a target Al/Si molar ratio of 0.0003, 0.001, 0.005, 0.01, 0.05, and 0.1. Reference samples without added $NaAlO_2$ were also synthesised for each Ca/Si series and equilibration time.

The synthesised samples underwent filtration in a glove box with a N_2 atmosphere after 1 day, 3 days, 7 days, 14 days, 28 days, 2 months, and 3 months of hydration for each target Ca/Si and Al/Si ratio. 2 samples of each series were stored as spare samples, and kept until the end of the project. During filtration, samples of the liquid phase were obtained by running 20 mL of solution through a syringe with a 45 μm filter membrane. The solids were filtrated and rinsed with a mixture of 50% absolute ethanol and 50% milliQ water, and then rinsed with absolute ethanol in order to remove the free water.

After filtration, the containers with the filtrated solids were placed in liquid nitrogen for 15 minutes, then dried in a freeze dryer for at least 48 hours. They were subsequently moved to a water vacuum dryer for at least 5 more days, to ensure that they were completely dried. The samples were then moved to a vacuum desiccator with a saturated solution of $CaCl_2*2H_2O$ in water, in order to obtain a relative humidity of 30%. Additionally, soda lime (Drägersorb 400) tablets were placed in the desiccator, in order to trap CO_2. After at least 14 days in the vacuum desiccator, the solid samples were ready to be analysed.

3.2 Reversibility

Samples with a Ca/Si molar ratio of 0.6, 0.8, 1.0, 1.2, 1.4, and 1.6 and an Al/Si molar ratio of 0.1 and 0 were synthesised. This was done the same way as described in Section 3.1, although with a total of 4 grams solids for the target Al/Si = 0.1 and a total of 8 grams solids for the Al/Si = 0. The total volume for the target Al/Si = 0.1 and 0 were 180 and 360 mL, respectively. After 10 days on a platform shaker with speed of 175 mot/minute, a 100 mM $NaAlO_2$ solution was added to the samples, in order to achieve a target Al/Si molar ratio of 0.1. The C-A-S-H and C-S-H samples were then shaken daily for another 28 days of hydration. After 28 days, the C-A-S-H samples were filtrated without washing, and subsequently placed back in their polyethylene containers. Solution from the C-S-H samples was added to achieve a W/S of 45. Thereafter, the C-A-S-H samples were shaken on a platform shaker at 175 mot/minute.

Samples of solution and solids were extracted after 6h, 1, 3, 7, and 21 days. On the day of sample taking, the polyethylene vessels with samples were stirred with a magnet stirrer to achieve homogeneity of solids and solution. Approximately 20 mL of each homogeneous mixture was pipetted into 50 mL centrifuge tubes and centrifuged at 4500 rpm for 4 minutes, in order to separate solids and solution. The solution was run through a syringe with a syringe filter of 45 μm and analysed by inductively coupled plasma optical emission spectrometry (ICP-OES). Additionally, solids were filtrated and dried as described in Section 3.1 for solid analysis by Fourier-transform infrared spectroscopy (FT-IR).

3.3 pH measurement

The pH of each sample solution was measured immediately after filtration, using a Mettler Toledo SevenMulti pH and conductivity meter. In order to minimise the sodium error, a calibration using NaOH concentrations of 0.1, 0.2, 0.5, and 1.0 M was performed. The measurements were corrected based on the calibration.

The Gibbs Free Energy Minimization (GEM-Selektor) software, version 3.8, was used to model pH in the samples, based on the weigh-in of the kinetics samples. In GEM-Selektor, the Debye-Hückel (Helgeson) model was used. The pH was calculated by the use of a process file within the GEM-Selektor software.

3.4 ICP-OES

Inductively coupled plasma optical emission spectrometry (ICP-OES) measures the concentration of ions in solution. This was used to determine the mass balance of the solid samples, and to determine the kinetics of the Al uptake in C-S-H. The ions were measured by ICP-OES with an Agilent ICP-OES 5110 apparatus. The samples were diluted with 2% HNO_3. Multi-standard solutions containing Al, Ca and Si were separately prepared in the same range of the expected concentrations in the samples to be measured (from 0 to 50 ppm).

3.5 XRD

XRD analyses were conducted on all solid samples, in order to determine the crystalline and amorphous phases present in the different samples with varying compositions. The XRD analyses on the references and on target Al/Si $\leq$ 0.01 were carried out on a PANalytical Empyrean diffractometer with an X-ray source of Cu-K_α ($\lambda = 1.5406\,\text{Å}$).The tension and current were 45 kV and 40 mA, respectively. For the incident beam path, a soller slit with 0.04 rad and mask size of 10 mm was used along with a $\frac{1}{8}°$ divergence slit and $\frac{1}{4}°$ anti-scatter slit. For the diffracted beam path, a soller slit with 0.04 rad and an anti-scatter slit with 8.0 mm were used.

Samples of each solid were prepared using an XRD sample preparation kit. The samples were run from an autosampler, and each measurement covered the range of 2θ =5–70° with a step-size of 0.0131°.

Samples with target Al/Si = 0.05 and 0.1 were measured at Empa with a different diffractometer and settings. The data was collected using a PANalytical X'Pert Pro MPD diffractometer equipped with rotating sample stage in a θ-2θ configuration with an X-ray source of Cu-K_α ($\lambda = 1.54\,\text{Å}$). The tension and current were 40 kV and 40 mA, respectively. For the incident beam path, a $\frac{1}{4}°$ divergence slit and $\frac{1}{2}°$ anti-scatter slit were used. each measurement covered the range of 2θ =5–70° with a step-size of 0.019°.

3.6 TGA

A selection of the solid samples were analysed by thermogravimetric analysis (TGA), in order to quantify water content and secondary phases present, for use in mass balance. The analyses were performed on a TA Instruments SDT 650 thermal analyser in Al_2O_3 crucibles. During analysis, the sample was kept in nitrogen by a nitrogen purge of $50\,\frac{\text{ml}}{\text{min}}$, and nitrogen protective pressure of $20\,\frac{\text{ml}}{\text{min}}$. The heating rate was kept at $20\,\frac{\text{K}}{\text{min}}$ until a temperature of 980°, before cooling to ambient temperature.

On each measurement, the derivative of the thermogravimetric (DTG) curve was calculated in order to observe changes in the weight loss, which indicate what phases and what quantities are lost at certain temperatures.

3.7 FT-IR

All solid samples were analysed by FT-IR, for the purpose of identifying and comparing the chemical groups present in samples with varying composition. The FT-IR analyses were run using a Bruker Tensor II FTIR spectrometer equipped with a platinum attenuated total reflectance (ATR) accessory. A small amount of powder from each solid sample was recorded between 4000 and 340 $cm^{(} - 1)$ with 32 scans. The data was treated with the Rubberband baseline correction tool in the Bruker OPUS software. Additionally, each dataset was normalised to the main peak at 940 cm^{-1} in Microsoft Excel before analysis.

3.8 Solid-state NMR

Samples with a Ca/Si ratio of 1.0 were analysed by solid-state ^{27}Al and ^{29}Si NMR analysis at Aarhus University, in order to investigate the local chemical environment of Al and the polymerisation of Si in C(-A)-S-H.

The^{27}Al MAS NMR spectra were recorded on a Varian Direct-Drive-600 spectrometer using a home-built CP/MAS probe for 4 mm outside diameter partially stabilised zirconia (PSZ) rotors. The^{27}Al MAS NMR analyses were run with a pulse width of 0.5 µs, spinning speed ν_R of 13.0 kHz, relaxation delay of 2 s, chemical shift reference of 1.0 $\frac{\mathrm{mol}}{\mathrm{L}}$ $AlCl_3 \cdot 6\,H_2O$ (aq), magnet strength of 600 MHz (14.09 T), spinning speed of 13 000 Hz. The Larmor frequency of the instrument was 156.223 MHz.

The ^{29}Si MAS NMR measurements were carried out on a Bruker-400 (9.39 T) spectrometer using a Bruker 1H-X 4 mm MAS probe for a spinning speed ν_R of = 10 kHz. The spectra used single-pulse excitation with a pulse length of 1.75 µs for an rf field strength of $\gamma\ \beta\ 1/2\ \pi = 71.4$ kHz, a recycle delay of 30 s, and 2560 scans. ^{29}Si chemical shifts are referenced to tetramethylsilane (TMS), using an external sample of β-Ca_2SiO_3 (larnite, Scawt Hill, N. Ireland) at -71.33 ppm as a secondary reference.

Results and Discussion 4

In this chapter, the results are presented in tables and figures. The results are divided into sections on the effect of Ca/Si, Al/Si, time, as well as reversibility, for a more comprehensible understanding of the results. In each section, there is a discussion on the results and the potential errors and uncertainties for each measurement are discussed.

The weigh-in of the kinetics and reversibility experiment are presented in Appendix A in Table A.2 and Table A.1, respectively. The mass balance of the samples is shown in Appendix C, which is used for several of the figures and in the discussion, e.g. for calculation of Ca/Si and Al/Si in C-S-H. Appendix D shows the concentration of elements measured by ICP-OES, and is used in all the figures containing information on aqueous concentration.

A summary of target Ca/Si and calculated Ca/Si in C-S-H is shown in Table 4.1. For the target Ca/Si of 0.6, mass balance calculations show that the actual Ca/Si in solids is 0.68 on average. For the other series, the target and calculated Ca/Si are closely correlated. However, as will be mentioned in the upcoming sections, Portlandite (CH) is detected in high Ca/Si, which may alter the Ca/Si present in C-S-H. Thus, it is more correct to reference the different Ca/Si as Ca/Si in solids, rather than in C-S-H.

Table 4.1: Target and average Ca/Si in solids, as well as the highest target Al/Si and calculated corresponding Al/Si in C-S-H.

Target Ca/Si	Ca/Si in solids	Target Al/Si	Al/Si in solids
0.60	0.68	0.100	0.089
0.80	0.81	0.100	0.087
1.00	1.00	0.100	0.090
1.20	1.20	0.100	0.085
1.40	1.40	0.100	0.094
1.60	1.59	0.010	0.002

Table 4.1 also shows the highest target Al/Si and corresponding Al/Si in solids after a hydration time of 60 days and 90 days, for Ca/Si $\leq$ 1.4 and Ca/Si = 1.6, respectively. For target Ca/Si = 1.6, the target Al/Si is 0.010, which is lower than for the other Ca/Si series, as target Al/Si of 0.1 were only synthesised for Ca/Si up to 1.4. For Ca/Si = 1.6, the calculated Al/Si in C-S-H is significantly lower than the

target Al/Si. This could be caused by carbonation of the $NaAlO_2$ solution used for the synthesis of the Ca/Si = 1.6, as ICP-OES results showed a lower concentration of Na than expected in the $NaAlO_2$ solution. Though, it is worth noting that the $NaAlO_2$ solution was exposed to air after the synthesis, and was only diluted by HNO_3 after several days of being exposed to air. It is thus possible that the actual Al/Si in the Ca/Si = 1.6 is higher than what the calculations indicate.

4.1 Effect of Ca/Si on C-S-H

Figure 4.1 shows the aqueous concentration of Si and Ca in solution for the reference samples, i.e. Al/Si = 0, after 28 days of hydration, plotted against the target Ca/Si of the C-S-H. The concentration of Si is plotted in the logarithmic scale, in order to distinguish better between the high Ca/Si, which have significantly lower concentrations of Si in solution. The concentration of Ca increases with increasing target Ca/Si, and the concentration of Si decreases with increasing target Ca/Si. Both trends in aqueous concentration can be explained partly by the target Ca/Si molar ratio itself. During synthesis, a higher ratio of Ca to Si is added to samples with a high target Ca/Si than to low Ca/Si. This means that the initial aqueous concentration of Ca will be relatively high and the aqueous concentration of Si will be relatively low. When C-S-H starts to form, both Si and Ca reacts from solution, and a lower aqueous concentration is thus found in solution. For high Ca/Si, it is probable that some Ca is left after the Si has reacted. For Ca/Si ≥ 1.2, some of the excess Ca might form Portlandite (CH).

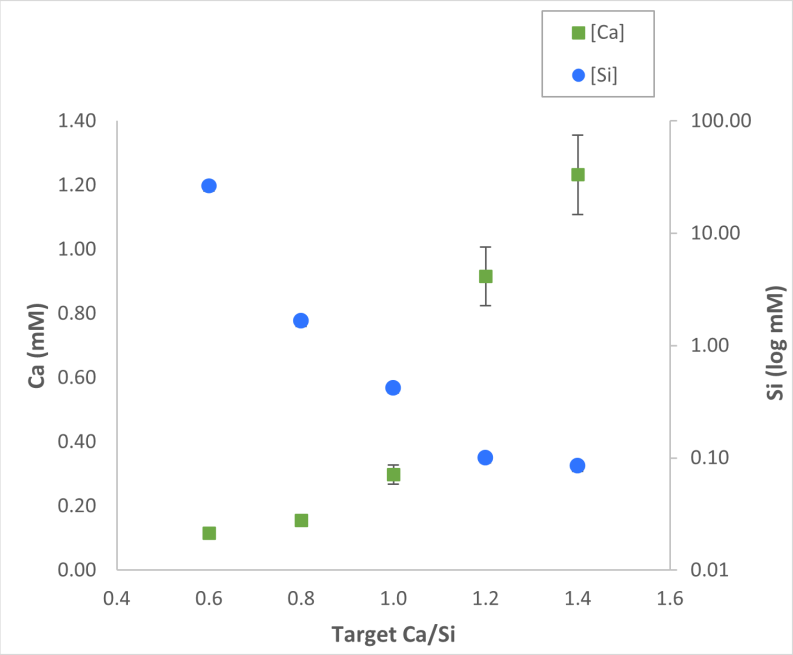

Figure 4.1: Aqueous concentration of Si and Ca in solution for Al/Si = 0 at a hydration time of 28 days.

The Na/Si molar ratio in the solids is plotted as a function of the Ca/Si molar ratio in the solids in Figure 4.2. Both the Na/Si and Ca/Si molar ratios are calculated based on mass balance. The Na/Si increases with decreasing Ca/Si, indicating that low Ca/Si has a higher uptake of Na in solids. Na^+ can act as a charge balancer in leu of cations with higher valence, such as Ca^{2+}. In low Ca/Si, there is less Ca^{2+} available to charge balance the C-S-H, and thus, Na^+ competes to charge balance the interlayer of C-S-H, together with the available Ca^{2+}.

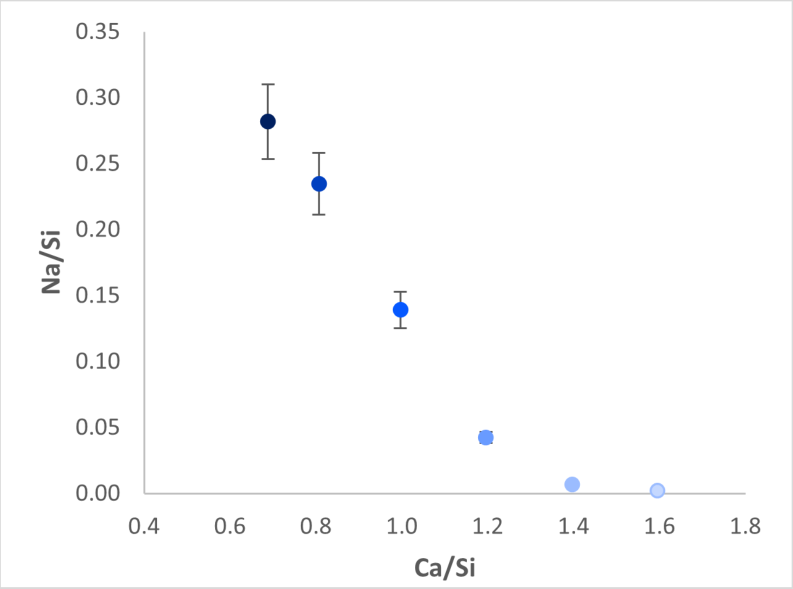

Figure 4.2: Change in Na/Si in solids as a function of Ca/Si in solids, from mass balance calculations.

The pH of each solution was measured to be between 13.3 and 13.5, increasing from the lowest target Ca/Si molar ratio of 0.6 to the highest target Ca/Si molar ratio of 1.6. After calibrating for alkali error, the measured values were corrected to be between 13.5 and 13.7. There were no differences in pH recorded within the same Ca/Si series, when only the first decimal of the pH was recorded, regardless of the Al/Si molar ratio. The modelled pH for target Al/Si = 0.1 ranged from 13.6 to 13.7. Figure 4.3 shows the comparison of the theoretical data for all the Ca/Si with a target Al/Si of 0.1 and experimental data of all the samples. As can be seen in Figure 4.3, there is a strong correlation between the theoretical and experimental data, although the pH values are not identical. The error for each measurement is 0.1, which signifies that the experimental and modelled values are overlapping.

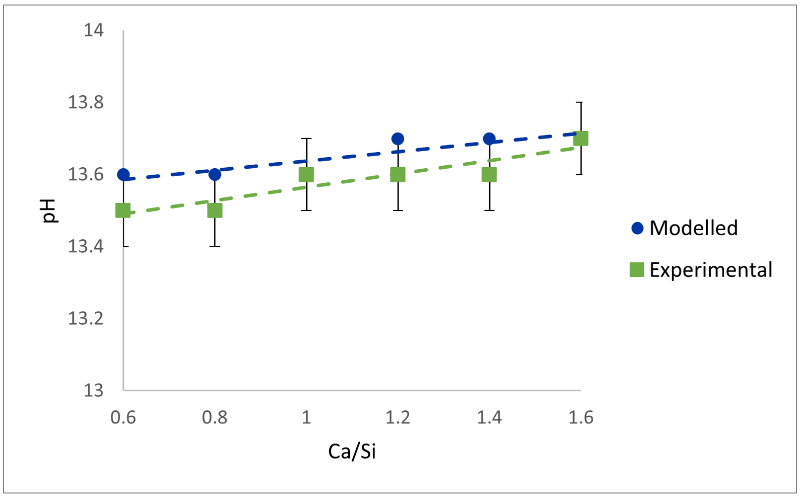

Figure 4.3: Comparison of pH results from experimental data of samples with target Al/Si from 0 to 0.1 and thermodynamic model CASH+ on the same data.

The high pH could be explained by the 0.5 M NaOH used for synthesis. The increase of pH with higher Ca/Si molar ratio was likely caused to by a higher OH- concentration in solution stemming from a higher ratio CaO, compared to the samples with lower Ca/Si molar ratios. However, the difference between the different Ca/Si molar ratios is small, and the pH is therefore mainly caused by the alkaline NaOH solution.

XRD diffractograms of the reference samples, i.e. Al/Si = 0, are shown in Figure 4.4. All the diffractograms contain C-S-H, which can be seen as bumps, rather than crystalline peaks. Additionally, the samples with a Ca/Si molar ratio ≥ 1.2 contain CH, which can be seen as the sharp crystalline peaks in Figure 4.4.

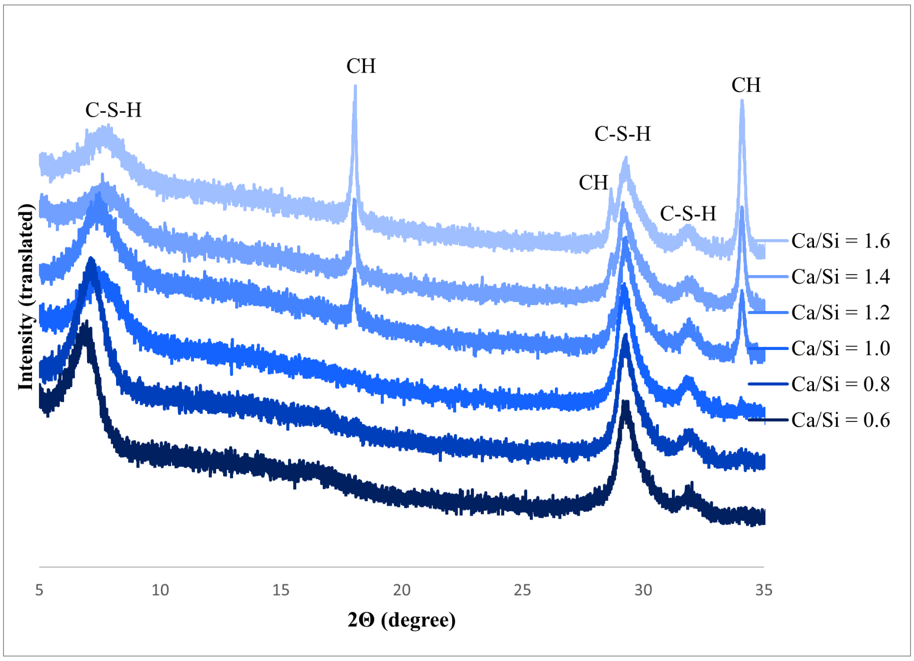

Figure 4.4: Reference samples (Al/Si = 0) after 28 days of hydration, measured by XRD. Graphs are translated along y-axis for clarity.

For Ca/Si ≥ 1.2, CH is present regardless of Al/Si molar ratio. The samples with a Ca/Si = 1.6 contain the highest amount of CH, and the content decreases with lower Ca/Si ratios. No CH or other secondary phases can be detected in the diffractograms of target Ca/Si ≤ 1.0. At 7 2θ, it can be seen that d002, i.e. the mean distance between the layers of C-S-H, moves to a higher 2θ with increased Ca/Si molar ratio. This shift indicates that the higher Ca/Si ratios have decreased basal spacing than the lower Ca/Si samples. The decreased basal spacing is likely caused by less H_2O in the interlayer of the C-S-H [7]. Additionally, the d002 is sharper for low target Ca/Si, which indicates a more ordered system, compared to the high Ca/Si.

Figure 4.5 shows the FTIR spectra of the 28 day reference samples. The bands are assigned to different chemical groups as shown in Table 4.2. Bending vibrations of O-Si-O groups in dreierketten chains and from water liberation can be seen from

400 to 800 cm^{-1}. The region between 800 and 1200 cm^{-1} is assigned to stretching vibrations of Si-O. [29]

The region from 500 to 800 cm^{-1} can be considered the fingerprint region, where changes in composition and topological features can be detected [29]. Bands ranging between 400 to 550 cm^{-1} are assigned to deformations of Si tetrahedra [28, 29], although the shoulder located at 480 cm^{-1} has a clear increase with increasing Ca/Si, which indicates that it is caused by a Q^1 signal [29]. At 660 cm^{-1}, a signal related to Si-O-Si bending and water liberation [29] can be seen. It increases slightly with decreasing Ca/Si, indicating a higher water content decreasing Ca/Si, which has also been suggested by the diffractograms presented in Figure 4.4. The band at 810 cm^{-1} is assigned to Si-O stretching of Q^1 sites [29], which is corroborated by its increase with increasing Ca/Si.

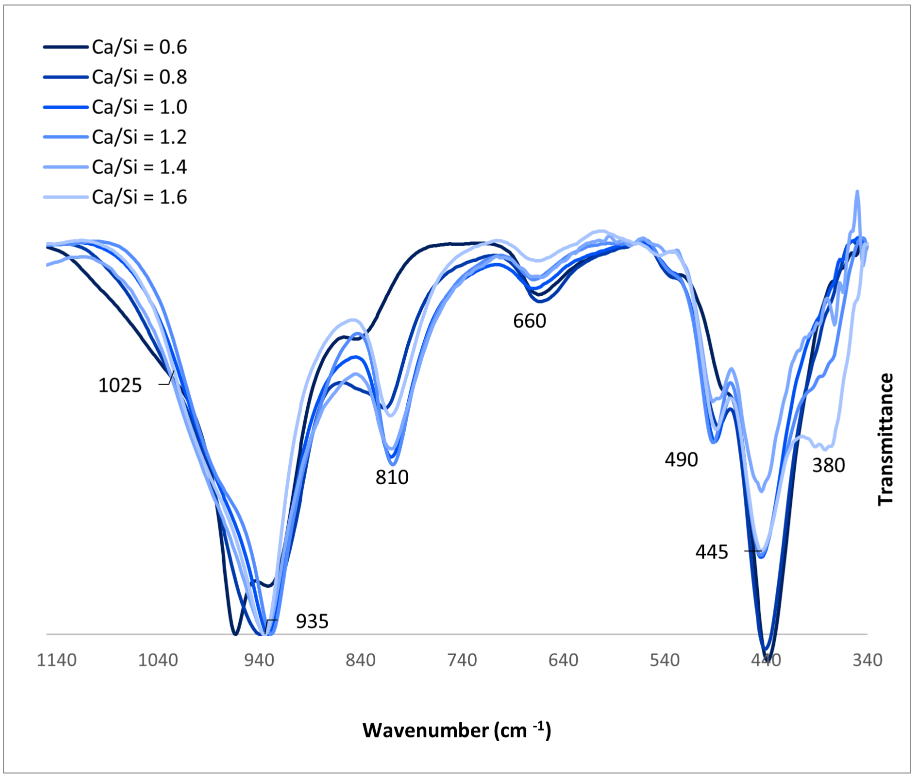

Figure 4.5: FT-IR spectra of reference samples with an equilibrium time of 28 days.

At 960 cm^{-1}, the main peak for C(-A)-S-H is located, which is associated with Si-O stretching [29]. With increasing Ca/Si, the peak shifts towards a lower wavenumber. This indicates a shorter mean chain length (MCL) of the C(-A)-S-H as it is depolymerised with increasing Ca/Si. The main peak at 935 cm^{-1} is often assigned to Q^2 sites [28, 30], but since it is predominant in all the C(-A)-S-H samples, it is believed to be caused by several vibrations, including a Q^2 signal at 935 cm^{-1} [29]. On the low-frequency side of the main peak, a shoulder can be located at approximately 930 cm^{-1} and is assigned to bridging Q^2 sites [29]. On the high-frequency side of the main peak, another shoulder can be located, at approximately 1025 cm^{-1}. It is also assigned to bridging Q^2 sites [29].

Table 4.2: Wavenumbers from reference samples and their assigned vibrational mode.

Wavenumber	**Assigned to**	**Interpretation**
420	δ Si-O	SiO_4 deformation
445	δ Si-O	SiO_4 deformation
490	δ Si-O-Si	SiO_4 deformation and Q^1 sites in C-S-H
660	δ Si-O-Si	Si-O-Si bending, water liberation
810	v Si-O	Q^1 sites in C-S-H
935	v Si-O	Q^2 sites in C-S-H
1150-1025	v Si-O	Q^2_b sites in C-S-H

To summarise, for C-S-H without Al, it was found that increasing Ca/Si leads to higher aqueous concentration of Ca and lower aqueous concentration of Si in solution at a given hydration time. The Na/Si molar ratio in the solids were found to increase with decreasing Ca/Si, as Na^+ acts as a charge balancer when there is less bivalent Ca^{2+} to charge balance the C-S-H. The pH in solution increases with increased Ca/Si, due to a higher content of alkaline Ca. C-S-H is observed in diffractograms of all the Ca/Si, and in Ca/Si ≥ 1.2, CH was also recorded. The basal spacing of the C-S-H increases with decreasing Ca/Si, indicating that less water is present in high Ca/Si compared to low Ca/Si. This was also confirmed by TGA. The presence of CH was corroborated by TGA, in which increasing amounts of CH and carbonation were found for increasing Ca/Si. FT-IR analysis indicated increased polymerisation for low Ca/Si, which means that the MCL increases.

4.2 Effect of Al/Si

The Al/Si in solids, as calculated by mass balance, are plotted against aqueous concentration of Al in target Ca/Si = 1.0 after 28 days of hydration, in Figure 4.6. There is a linear trend between aqueous concentration and Al/Si in solids. With increasing target Al/Si, there is an increasing calculated Al/Si in solids after 28 days of hydration.

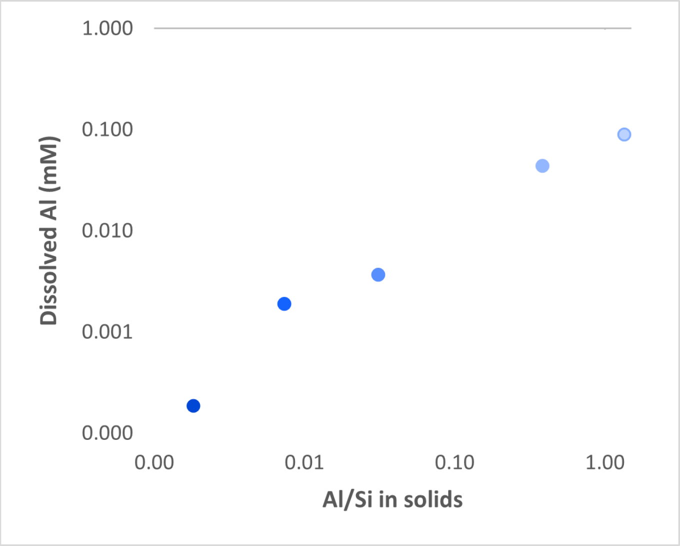

Figure 4.6: Calculated Al/Si in solids against aqueous concentration of Al, in target Ca/Si = 1.0 with a 28 day hydration time.

Figure 4.7 shows the diffractograms of target Ca/Si = 1.0 with a hydration time of 28 days, and varying target Al/Si. With increasing target Al/Si, the d002 peak shifts towards a lower 2θ, indicating an increased basal spacing with higher Al/Si. The increased basal spacing could be caused by the increase of Al/Si, as Al(IV) binds to two pairing silicate tetrahedra, and thereby forms longer mean chain lengths (MCL) in the C-S-H. The shift towards a lower 2θ with increasing Ca/Si can best be seen in the difference between Al/Si = 0 compared to target Al/Si = 0.05 and 0.1.

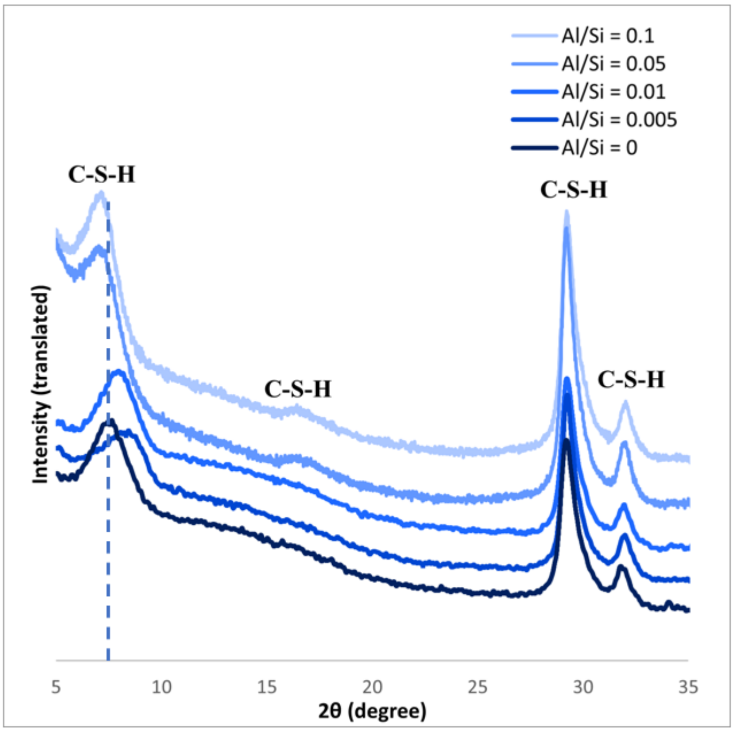

Figure 4.7: Diffractograms of target Ca/Si = 1.0 and varying target target Al/Si, with a hydration time of 28 days. Target Al/Si = 0.005 and 0.01 have a hydration time of 90 days.

The FT-IR spectra of target Ca/Si = 1.0 and increasing Al/Si are shown in Figure 4.8. As with the reference samples shown in Figure 4.5, bending vibrations are shown in the region from 800 to 400 cm^{-1}, while stretching vibrations are found between 1200 and 800 cm^{-1}. The regions are discussed in more detail in Section 4.1, while the differences related to Al/Si will be discussed in this section.

With increasing Al/Si, the band assigned to SiO_4 deformation at 445 cm^{-1} increases in transmittance, while the bands assigned to Q1 at 490 and 810 cm^{-1} decrease. This indicates a more polymerised system and thus longer mean chain length (MCL) for higher Al/Si in C-S-H. Additionally, the main signal at 940 cm^{-1}, assigned to several vibrations of both Q^1 but mainly Q^2 sites [29, 31], shifts towards a higher wavenumber with increasing Al/Si, further corroborating the increase of MCL.

The shoulder at 1025 cm^{-1} is assigned to symmetric bending of Al-O-H and increases in intensity with increasing Al/Si, indicating an increasing presence of Al in C-S-H [27]. At 880 cm^{-1}, a shoulder assigned to stretching vibrations of Al-O-Si (terminal bond) [27, 32] can be seen. When comparing the target Al/Si between 0.01 and 0.1, this band is increasing in intensity with increasing Al/Si. This further substantiates the increasing presence of Al with increasing Al/Si.

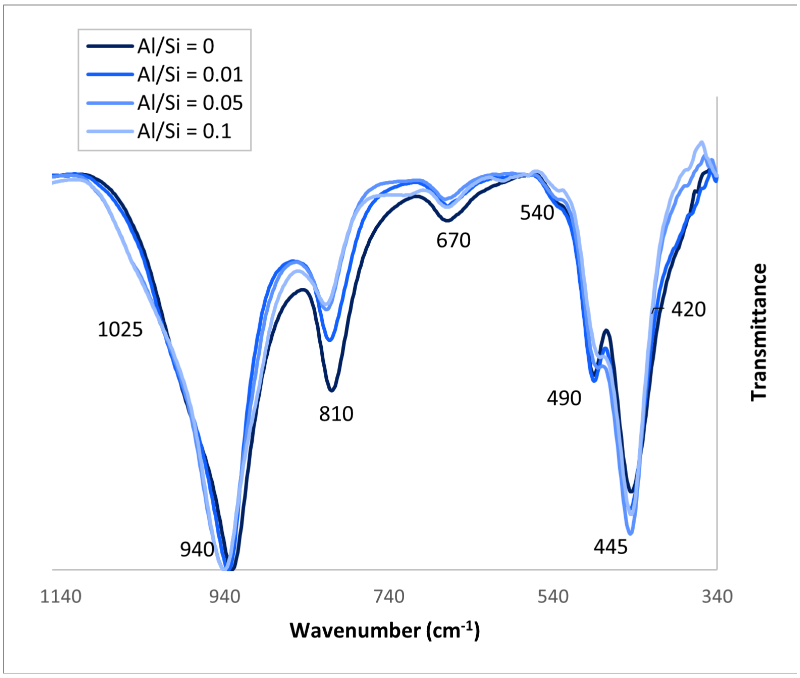

Figure 4.8: FTIR spectra of target Ca/Si = 1.0 with a varying target Al/Si, with a 28 day hydration time.

The water liberation at 670 cm^{-1} decreases slightly between Al/Si = 0 and the samples with higher Al/Si. Although, when comparing the transmittance for target Al/Si between 0.01 and 0.1, there is a slight increase with increasing Al/Si. The shoulder at the high-frequency side of the main peak, at approximately 1025 cm^{-1}, is assigned to bridging Q^2 sites [29]. It is increasing with increasing Al/Si, notably so for target Al/Si = 0.1. Thus, with an increase of Al/Si, the MCL is increasing as more Q^2 and less Q^1 is formed in the C(-A)-S-H.

Table 4.3: Wavenumbers from samples with increasing Al/Si and their assigned vibrational mode.

Wavenumber	Assigned to	Interpretation
420	δ Si-O	SiO_4 deformation
445	δ Si-O	SiO_4 deformation
490	δ Si-O-Si	SiO_4 deformation and Q^1 sites in C-S-H
660	δ Si-O-Si	Si-O-Si bending, water liberation
810	v Si-O	Q^1 sites in C-S-H
880	v Al-O-Si	Terminal bond
935	v Si-O	Q^2 sites in C-S-H
1150-1025	v Si-O and Al-O-H	Q_b^2 sites in C-S-H and C-A-S-H

To summarise, with increasing Al/Si, there is an increase of polymerisation and thus mean chain length (MCL), as aluminium tetrahedra occupy the bridging sites of C-S-H. The increase in MCL can be seen in FT-IR spectra, where a clear decrease of Q^1 and increase of Q^2 bands can be seen with increasing Al/Si. Furthermore, XRD diffractograms indicate that an increase of Al/Si increases the basal spacing in the C-S-H, which in turn indicates that more water is present in the interlayer with increasing Al/Si.

4.3 Effect of Ca/Si on C-A-S-H

Figure 4.9 shows the concentration of Al in solution for Ca/Si between 0.6 and 1.4 and Al/Si = 0.1, with a total hydration time of 28 days since the addition of $NaAlO_2$. The concentration of Al in solution decreases as the Ca/Si increases. This indicates that more Al is taken up in the solids of the high Ca/Si, compared to the low Ca/Si. Presumably, C-A-S-H is then formed.

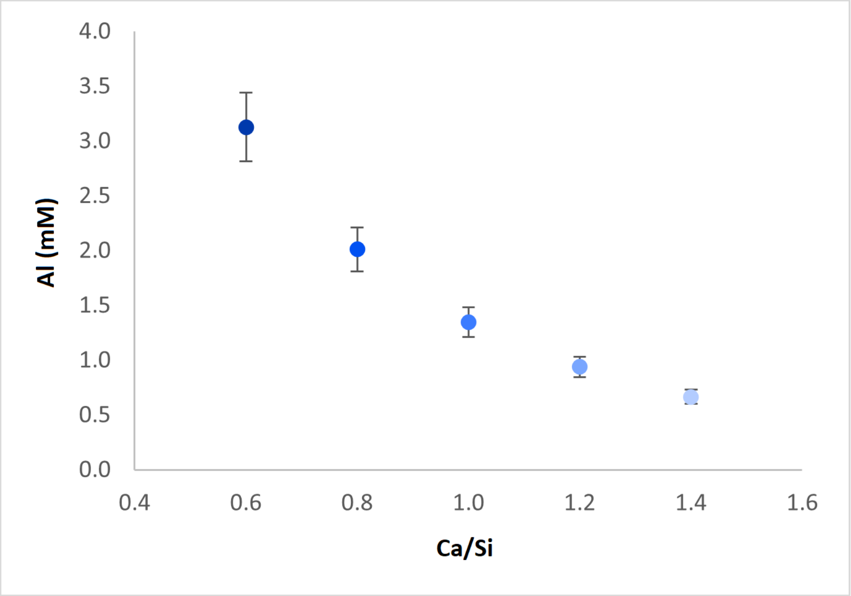

Figure 4.9: Concentration of Al in solution for Ca/Si between 0.6 and 1.4 and Al/Si = 0.1, with a hydration time of 28 days.

The calculated Al/Si in solids after 28 days of hydration is plotted against dissolved Al concentration in solution in Figure 4.10. The Al/Si in solids increases with increasing Ca/Si, indicating that the kinetics of Al uptake is higher with increasing Ca/Si C-S-H. Near all the Al has been taken up in high Ca/Si solids after 28 days, while some Al is left in solution for low Ca/Si at the same hydration time.

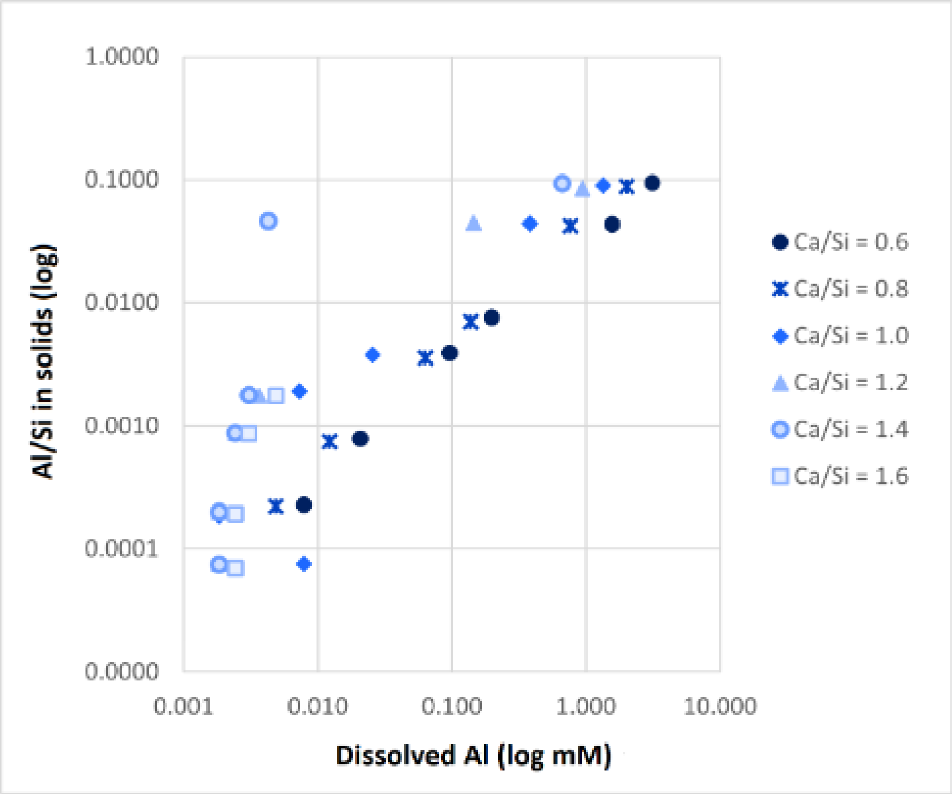

Figure 4.10: Mass balance calculation of Al/Si in solids after a hydration time of 28 days. The results are plotted in the logarithmic scale, in order to distinguish better between Ca/Si series.

Figure 4.11 shows the calculated Na/Si in C-A-S-H against the calculated Ca/Si in C-A-S-H for samples with a hydration time of 28 days. At this point, the C-A-S-H should be at semi equilibrium. The Na/Si molar ratio decreases with increasing Ca/Si, and the Ca/Si $\geq$ 1.1 contains little to no Na. In low Ca/Si, there is less Ca^{2+} in solution when C(-A)-S-H is formed. Ca^{2+} helps to charge balance the C(-A)-S-H, and as a divalent cation, it is preferred over monovalent cations, such as Na^{+}. However, in leu of excess Ca^{2+}, the C(-A)-S-H can be charged balanced by Na^{+}. Thus, it is logical that low Ca/Si has a higher uptake of Na^{+} than high Ca/Si.

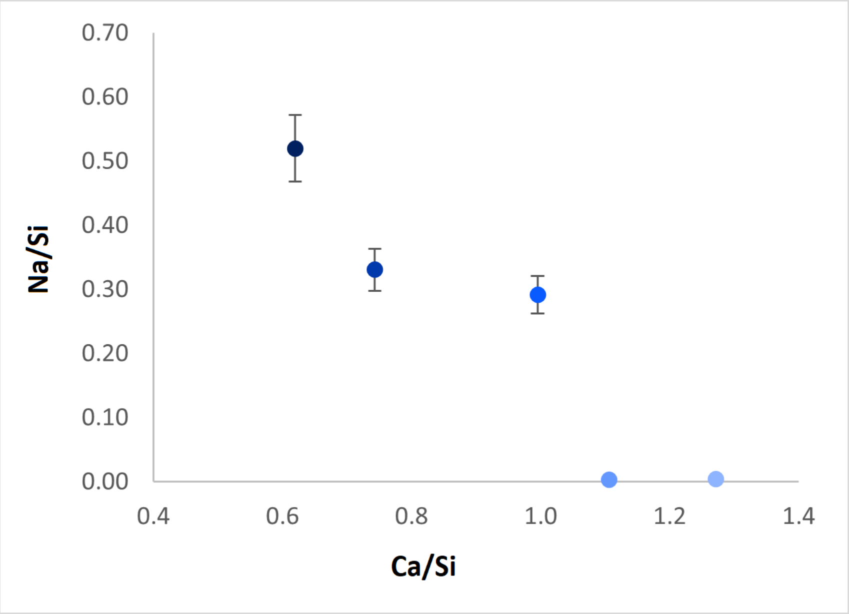

Figure 4.11: Calculated Na/Si in solids plotted against calculated Ca/Si in solids in samples containing target Al/Si = 0.1.

The concentration of Si and Ca in solution for target Al/Si = 0.1 and a hydration time of 28 days are shown in Figure 4.12. The concentration of Si is decreasing and the concentration of Ca is increasing with increasing Ca/Si. The decrease of Si can be explained directly through the Ca/Si molar ratio, as low Ca/Si samples have a higher relative amount of Si compared to Ca, and therefore will have more Si in solution. High Ca/Si samples have a higher relative amount of Ca compared to Si. As the lowest Ca/Si synthesised is 0.6, and the lowest commonly known C(-A)-S-H is 0.66, it is reasonable to believe that some of the Si is available in solution even as all the Ca is used up in solids, and thus the Si concentration will stay high compared to higher Ca/Si. When C-S-H is formed, Ca and Si is gradually reacting from solution and into solids, with different Ca/Si compositions. In high Ca/Si, the amount of Ca is relatively higher than Si, and during the formation of C-S-H, it is plausible that the Si has been fully reacted before the Ca. Thus, a higher concentration of Ca is left in solution at (semi)equilibrium.

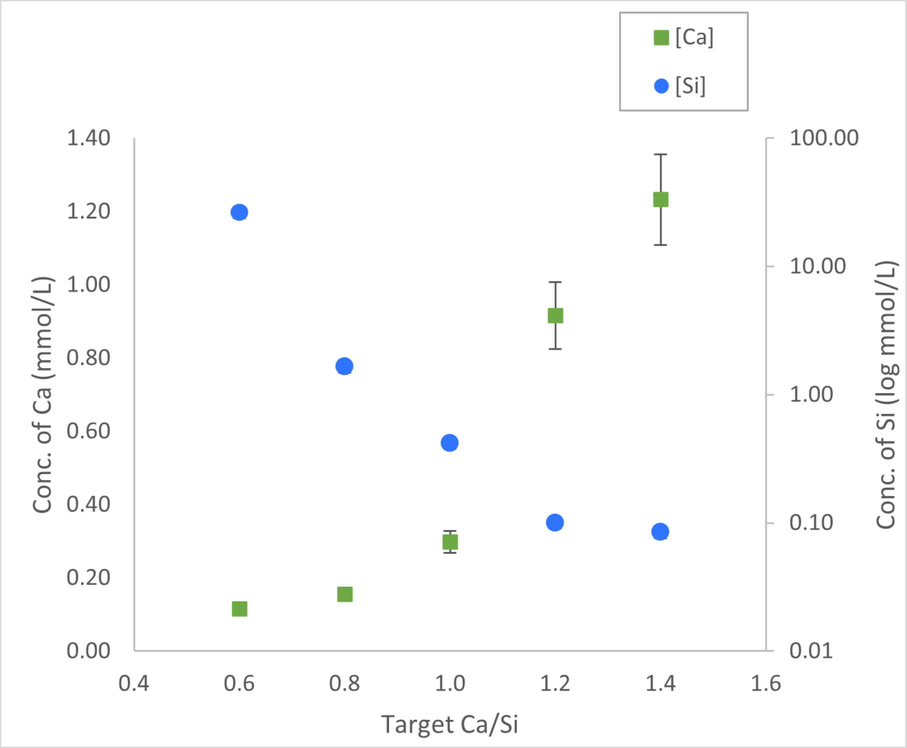

Figure 4.12: Concentration of Si and Ca in solution for Ca/Si between 0.6 and 1.4 and Al/Si = 0.1, with a hydration time of 28 days. Note that the concentration of Si is expressed in the logarithmic scale, in order to distinguish better between high Ca/Si.

Figure 4.13 shows the diffractograms of target Al/Si = 0.1 for varying target Ca/Si with a 28 day hydration time. The low Ca/Si samples show the presence of C(-A)-S-H, while secondary phases are present in the Ca/Si ≥ 1.2. The secondary phases present are CH, monocarbonate (Mc, $C_3A \cdot CaCO_3 \cdot 11\,H_2O$) and hemicarbonate (Hc, $C_3A \cdot 0.5\,Ca(OH)_2 \cdot 0.5\,CaCO_3 \cdot 11.5\,H_2O$). Mc and Hc are not detected in target Al/Si ≤ 0.05. The presence of Mc, Hc and CH should be accounted for when discussing the results on target Al/Si = 0.1 for target Ca/Si ≥ 1.2, as the presence of secondary phases affects the composition of the C(-A)-S-H.

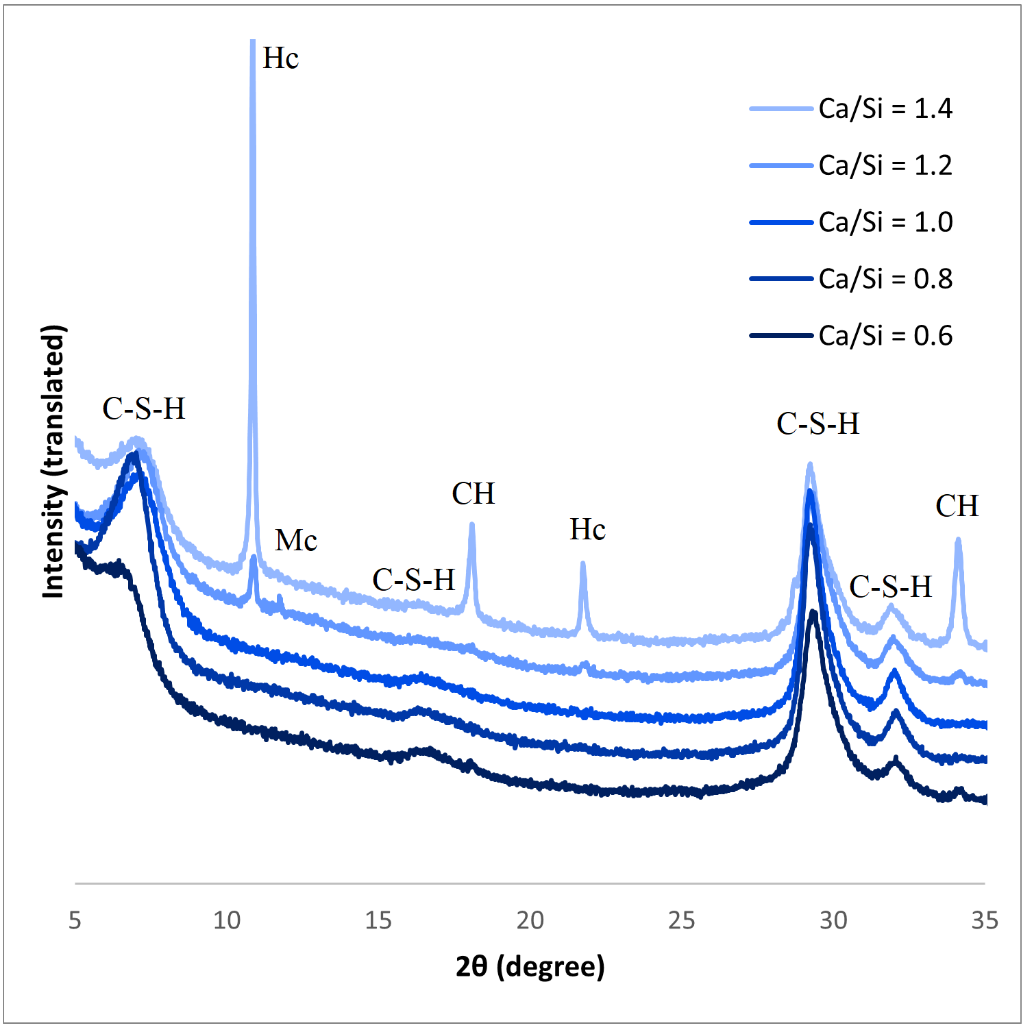

Figure 4.13: Diffractograms of target Al/Si = 0.1 and hydration time of 28 days.

FTIR spectra of target Ca/Si = 0.6 and 1.0 and target Al/Si = 0 and 0.1 after 28 days of hydration are shown in Figure 4.14. A general discussion of the vibrational and stretching modes of C-S-H and C-A-S-H can be found in Section 4.1 and Section 4.2 and in Table 4.2 and Table 4.3. The discussion below compares target Al/Si of 0 and 0.1 and target Ca/Si = 0.6 and 1.0.

The bands assigned to Q1 at 490 and 810 cm^{-1} decrease with increasing Al/Si for both the target Ca/Si = 0.6 and 1.0, indicating a longer mean chain length (MCL). The spectra shift towards a higher wavenumber in the target Al/Si = 0.1, which is most apparent in the main peak at 940cm^{-1}, assigned to several vibrations of both Q^1 but mainly Q^2 sites in C-S-H. [29, 31]

This is further confirmation of the increase of MCL in the presence of Al, as Al tetrahedra occupy the bridging sites of the C-S-H and thus links dimers of silicate tetrahedra together in a dreierketten chain. The shoulder at 1025 cm^{-1} is assigned to symmetric bending of Al-O-H [27] and shows a clear shift towards a higher wavenumber in the samples with target Al/Si = 0.1. The shoulder at 880 cm^{-1}, which is assigned to stretching vibrations of Al-O-Si (terminal bond) [27,32] can be detected, although the change in intensity does not increase in the presence of Al the same way as shown in 4.8. This does not counter indicate that Al is present in C-S-H, as the peak could be hidden behind other bands, and furthermore, since other bands show a clear trend with increasing Al/Si.

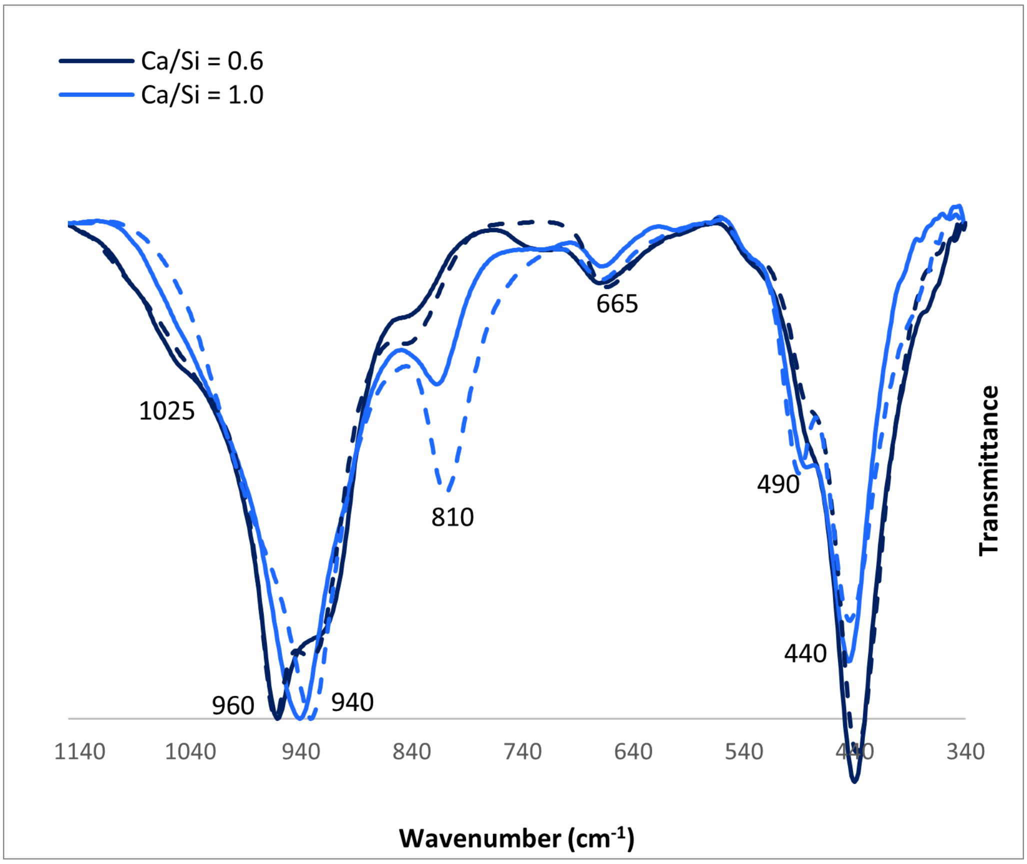

Figure 4.14: FTIR spectra of target Al/Si = 0.1 and 0 with a hydration time of 28 days. Important peaks are labeled. Stipled line; Al/Si = 0, solid line; target Al/Si = 0.1.

Results from thermogravimetric (TG) and derivative thermogravimetric (DTG) analyses of varying Ca/Si with target Al/Si = 0.1 and hydration time of 28 days are shown in Figure 4.15. Target Ca/Si = 1.4 contains CH, while the lower Ca/Si do not, which is consistent with the XRD measurements. The carbonation is kept relatively stable at less than 1 wt%. Weight loss from Hc and Mc happens simultaneously with the weight loss for water in C-S-H [33]. As Hc and Mc were detected by XRD in Ca/Si = 1.4 and target Al/Si = 0.1, some of the weight loss assigned to C-S-H is probably caused by these secondary phases. Thus, there seems to be a trend with increasing amounts of water loss by C-S-H in increasing Ca/Si, in a more clear way than shown in Figure 4.15. This is consistent with the results from XRD, where an increased basal spacing was recorded with decreased Ca/Si, which allows for more water to occupy the interlayer of the C-S-H.

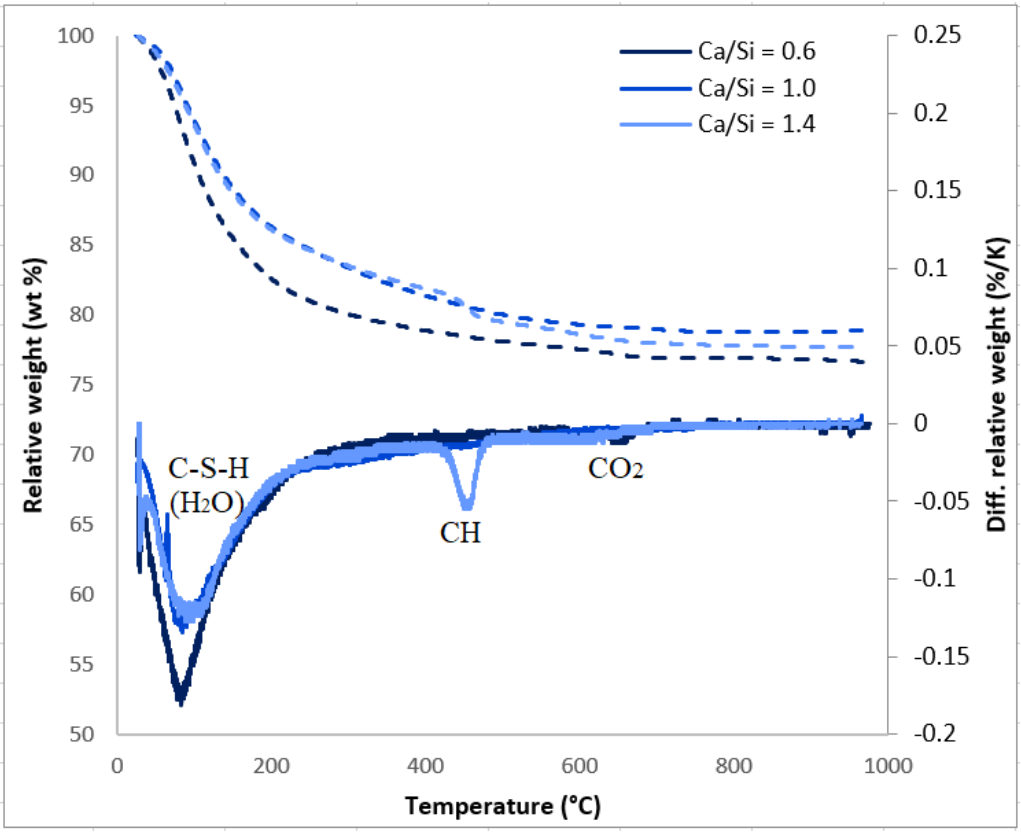

Figure 4.15: Thermogravimetric analysis of target Al/Si = 0.1 samples with 28 days of hydration. The dotted graphs show the weight loss of samples against time, while the solid lines show the differential weight change of the samples.

In summary, the effect of Ca/Si on C-A-S-H is such that an increased Ca/Si increases the uptake of Al into solids. Mass balance calculations show a clear trend, where low Ca/Si has a lower Al/Si in solids compared to high Ca/Si at a hydration time of 28 days. The presence of Al in C-S-H is detected by FTIR, which also shows an increased mean chain length (MCL), as Al is taken up in the bridging sites between silicate tetrahedra. Uptake of Na in solids increases as Ca/Si decreases, in samples with target Al/Si = 0.1, indicating that Na charge balances low Ca/Si. The concentration of Si and Ca in solution follows the same trend as for the reference samples, with an increasing concentration of Ca and decreasing concentration of Si with increasing target Ca/Si. In target Ca/Si $\geq$ 1.2 and target Al/Si = 0.1, monocarbonate and hemicarbonate are present in the solids.

4.4 Effect of time

The change of aqueous concentration of Si and Ca over time are shown in Figure 4.16 and Figure 4.17, respectively. The concentration of Si in Ca/Si = 1.0 and Al/Si = 0 is relatively stable over time, with overlapping values. For Ca/Si = 1.0 and target Al/Si = 0.1, there is an initial increase in concentration of Si, but after 7 days, the concentration in solution is decreasing.

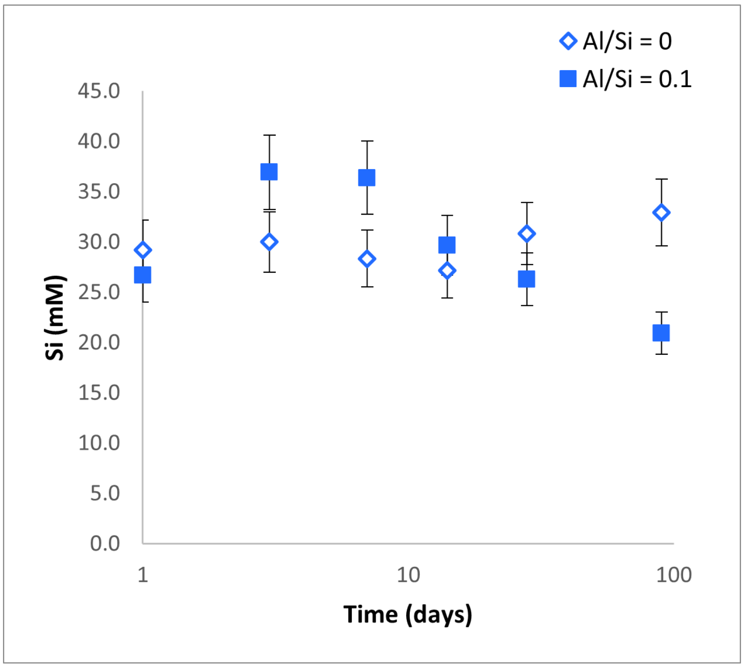

Figure 4.16: Change of aqueous concentration of Si with time. The axes are shown in the logarithmic scale, for clarity. Blank circles; references (Al/Si = 0), filled circles; target Al/Si = 0.1.

In Figure 4.17, it is clear that the aqueous concentration of Ca changes over time for target Ca/Si = 1.0. In the Al/Si = 0, the aqueous concentration increases initially, but decreases slightly in in the 90 day hydration sample. Although, the concentrations are overlapping when the measurement error of 10% is accounted for. For target Al/Si = 0.1, the trend is more clear. There is a decrease of aqueous Ca concentration with time, indicating that Ca is taken up in the C(-A)-S-H, presumably as Ca^{2+} in the interlayer, or as the C(-A)-S-H rearranges and changes stoichiometry. As the concentration of Si in the target Al/Si = 0.1 also decreases with higher hydration times, it suggests that more C(-A)-S-H is formed.

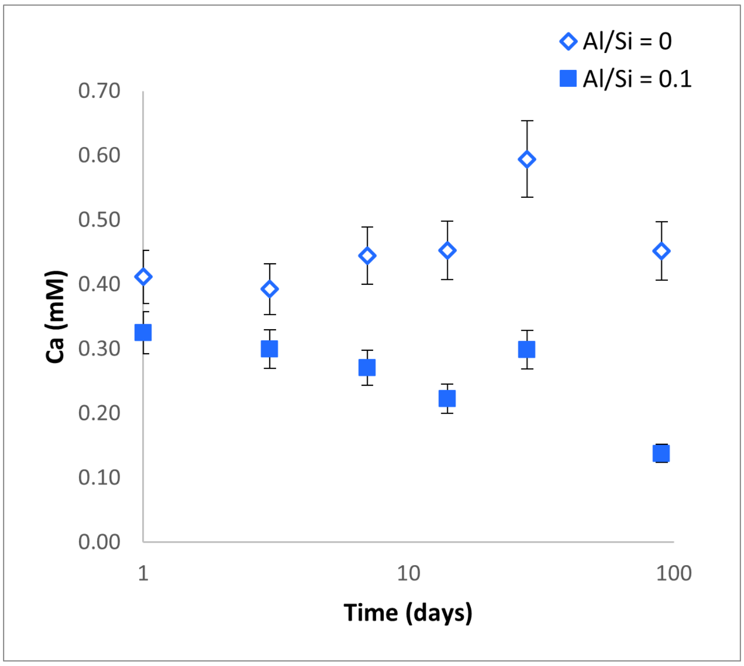

Figure 4.17: Change of aqueous concentration of Ca with time. The axes are shown in the logarithmic scale, for clarity. Blank circles; references (Al/Si = 0), filled circles; target Al/Si = 0.1.

The change in aqueous concentration of Al for target Al/Si = 0.1 with increasing hydration time is shown in Figure 4.18. The aqueous concentration decreases with increasing hydration time for all Ca/Si series, indicating that Al is taken up in C-S-H, and that C-A-S-H is formed. For the lower Ca/Si series, there is an increasing concentration of Al in solution, which means that less Al has been taken up into the C-S-H in these samples. Thus, the change in aqueous concentration of Al indicates that kinetics for Al uptake in high Ca/Si is faster than in low Ca/Si.

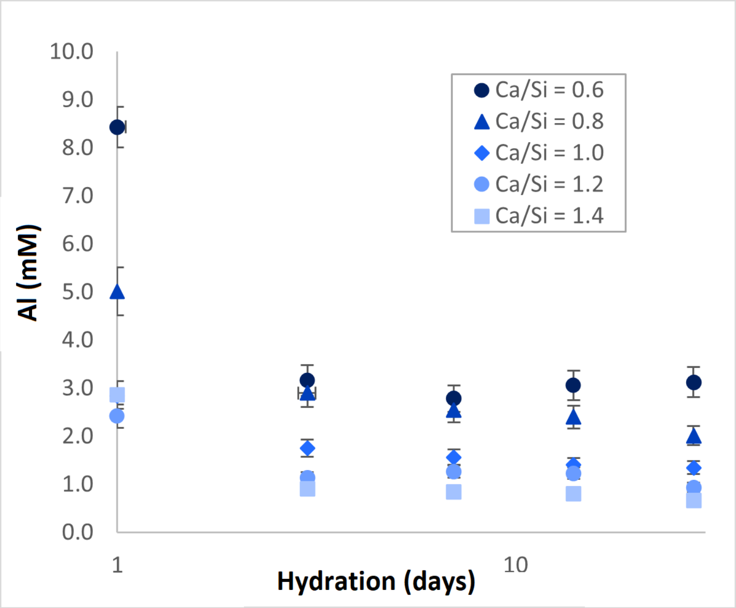

Figure 4.18: Change of aqueous concentration of Al with time.

Diffractograms of Ca/Si = 1.0 and target Al/Si = 0.1 with varying hydration times are shown in Figure 4.19. For increasing hydration time, there is a shift in d002 towards a lower 2θ, indicating an increase in basal spacing. The increase in basal spacing suggests an increase of water in the interlayer of the C-S-H, but could also be caused by an increase of Al in the interlayer, as an effect of higher Al uptake with time. Additionally, the d002 becomes increasingly sharper with increasing hydration time, indicating a more ordered structure of the C-S-H. Interestingly, the 28 day sample shows a less sharp d002 than the 14 day and 60 day samples, indicating that it is less ordered than those samples. However, the change in the d002 peak should be considered carefully, as it can change slightly depending on the measurements.

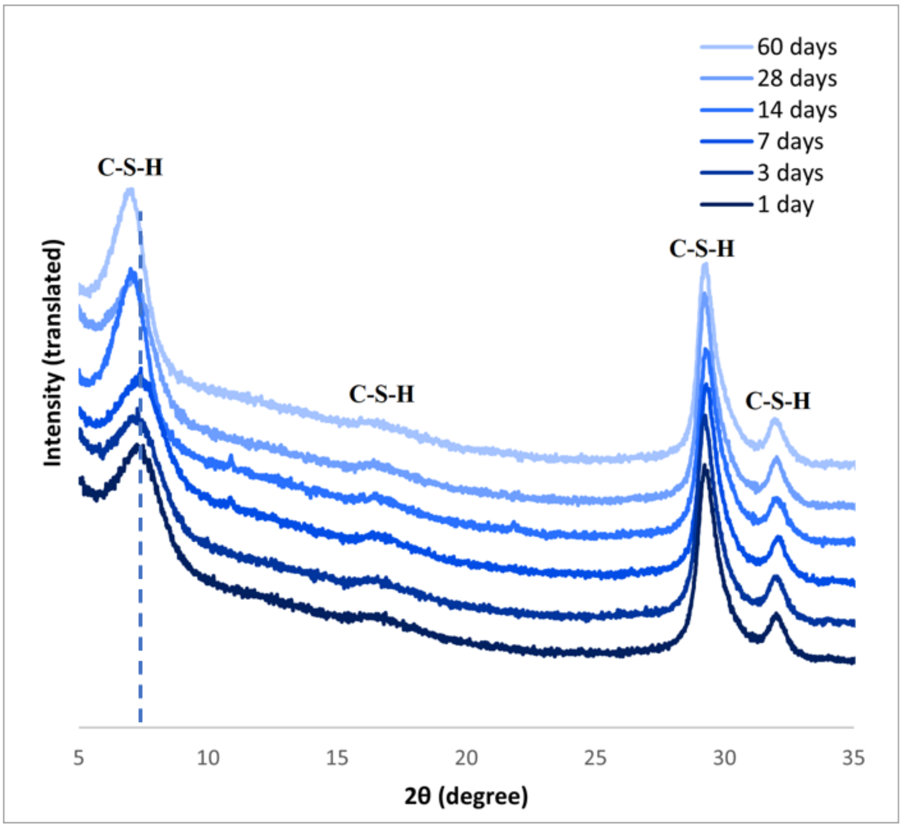

Figure 4.19: Diffractograms of Ca/Si = 1.0 and target Al/Si = 0.1 with varying hydration time. Intensities are translated along y-axis for clarity.

Figure 4.20 shows the thermogravimetric analysis (TGA) and differential thermogravimetric results (DTG) of target Ca/Si = 1.0 with a target Al/Si = 0.1 and with a hydration time of 3, 14, 28 and 60 days. The weight loss between 30°C and 600°C can be attributed to water loss of C-S-H, after weight loss from potential secondary phases has been subtracted [29]. In this case, the weight loss can be attributed to the water loss of C(-A)-S-H, as the uptake of Al has been confirmed by decreasing Al concentrations in solution, and as no secondary phases have been detected in the diffractograms of target Ca/Si = 1.0. Between 400 and 520°C, there is a weight loss reminiscent of that of CH [29, 33]. However, as no secondary phases were detected by diffractograms, it is considered as loss of water from C(-A)-S-H. Additionally, there is a small weight loss at approximately 700°C, which comes from carbonation, i.e. $CaCO_3$ [33]. Carbonation from $CaCO_3$ indicate that the samples have been exposed to CO_2, likely from storage and synthesis. The glove box used for synthesised was not checked for leaks before use, and it is possible it did not have a sealed atmosphere without CO_2. During storage in desiccators, the samples were exposed to air several times, during and between analyses, and the vacuum system was not ideal, so it was likely for some air to penetrate the vacuum during storage. Thus, the carbonation can be explained by poor handling and storage.

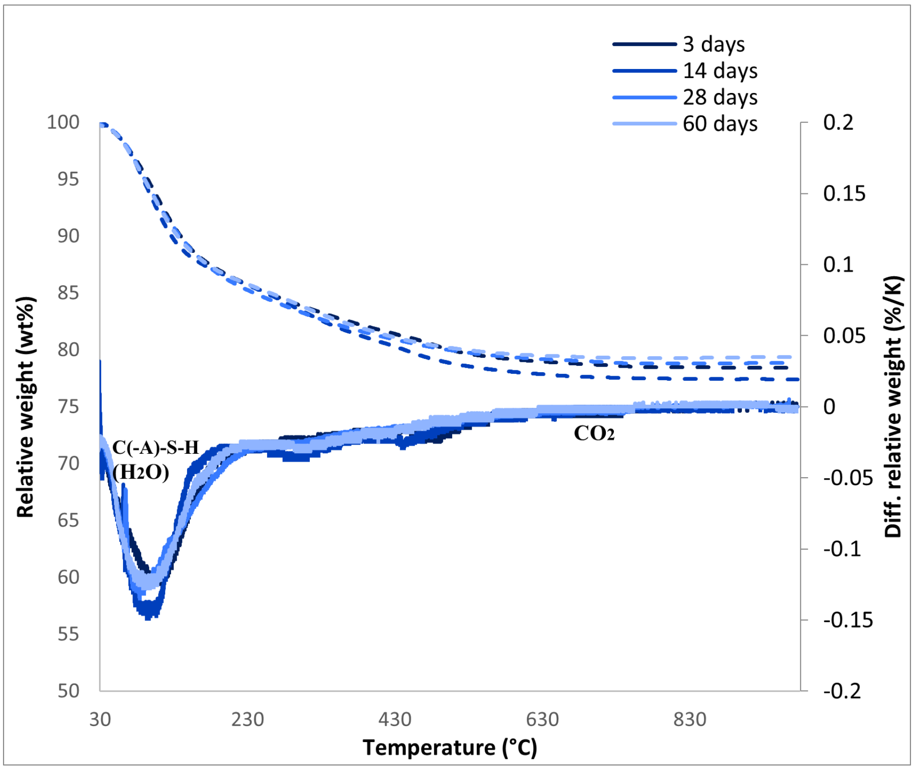

Figure 4.20: Thermogravimetric analysis of Ca/Si = 1.0 and target Al/Si = 0.1 samples from 3, 14, 28 and 60 days of hydration. The dotted graphs show the weight loss of samples with increasing temperature, while the solid lines show the differential weight change of the samples.

The water content in solids of Al/Si = 0.05 and varying hydration time is shown in Figure 4.21. Although the measurement error overlaps several of the results, there is a general trend of more H_2O present in the low Ca/Si compared to high Ca/Si. This trend can also be seen in the XRD diffractograms in Figure 4.4, where d002 shifts towards a lower 2θ for decreasing Ca/Si, indicating increased basal spacing.

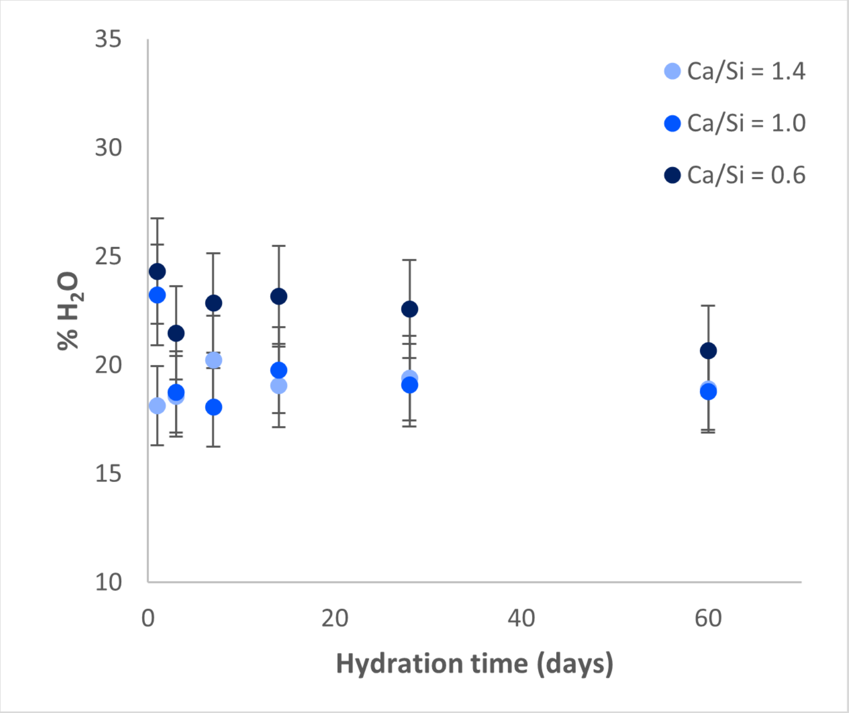

Figure 4.21: Water content in solids with Al/Si = 0.05 and varying hydration time.

The ^{29}Si NMR spectra of target Ca/Si = 1.0 (C-A-S-H) and target Al/Si = O (C-S-H) with increasing hydration times are shown in Figure 4.22. The C-S-H spectra have two main peaks at approximately -79 and -85 ppm, which are assigned to Q^1 and Q^2 sites of the dreierketten silicate chains, respectively [25, 34]. The Q^2 resonance has contributions from both pairing and bridging sites, Q^2p and Q^2b, which resonate at approximately -85 and -83 ppm in the spectra of C-S-H [25]. The peak for Q^1 sites at approximately -79 ppm shifts towards a lower chemical shift in both the C-S-H and C-A-S-H spectra with increasing hydration time, indicating a change in local environment for the Si.

For the ^{29}Si NMR spectra with target Al/Si = 0.1 (C-A-S-H), there is an additional peak between the Q^1 and Q^2 sites. These resonances are not resolved for the Al/Si = 0.1, as there is a partial overlap between the Q^2 peak and the peak for Q^2_p(1Al) site in C-S-H [25, 35]. If Al is in the Q^2_p(1Al) site, it means that it is a bridging tetrahedra between to silicate tetrahedra in C-S-H. Thus, Figure 4.22 confirms the presence of Al in C(-A)S-H, where Al is assigned to be bound in a bridging position between two pairing Q^2 silicate tetrahedra.

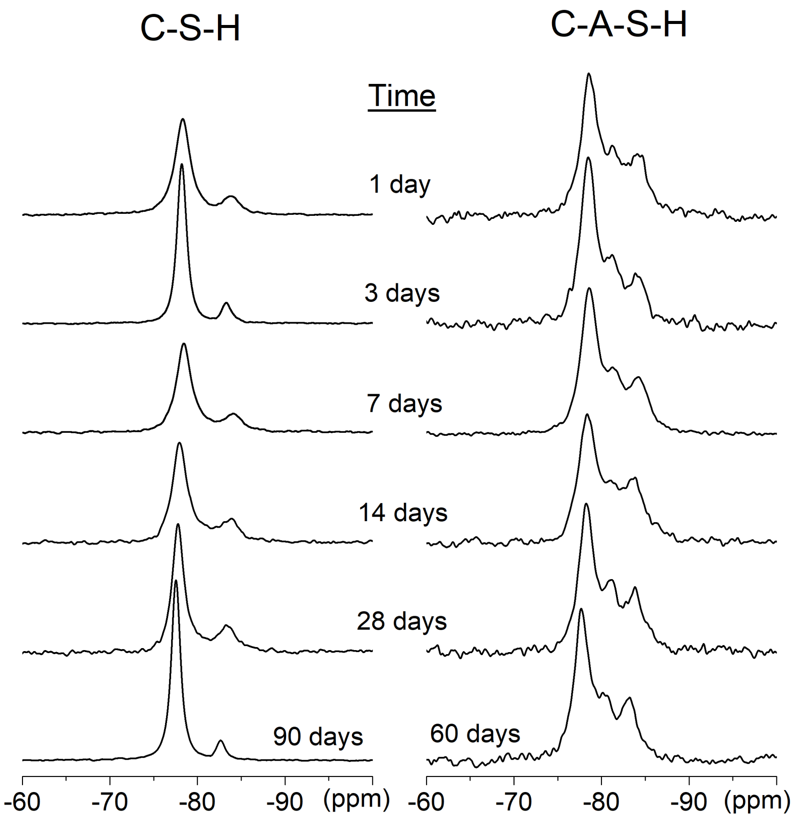

Figure 4.22: ^{29}Si NMR analysis of samples with Ca/Si = 1.0 and target Al/Si = 0.1 with different hydration time.

Figure 4.23 shows the ^{27}Al NMR spectra of the Ca/Si = 1.0 and target Al/Si = 0.1, with different hydration times. In the ^{27}Al NMR spectra, there are resolved resonances from tetrahedral coordination of Al at 50-80 ppm and octahedral coordination of Al at 0-20 ppm. The tetrahedral resonances at 74 and 68 ppm are assigned to Al(IV) in bridging sites of the silicate chains [25].

Al is observed to be incorporated in the bridging sites of the silicate structure by both the Al(IV) resonances in the ^{27}Al NMR spectra and by the Q^2_p(1Al) peak in the ^{29}Si NMR spectra.

All the samples contain a high ratio of Al(IV) and a lower ratio of Al(V) and Al(VI), regardless of hydration time. The quantification of the different Al species is summarised in Table 4.4. There is a general increase of Al(VI) with increasing hydration time, together with a decrease of Al(IV) and a rather stable amount of Al(V). It is worth noting that the sample at 28 days does not follow this trend. The low percentage of Al(V) has been seen in other studies, although the content from 1.5 % to 4.4 % in these samples is lower than other studies, which often report quantities of 5-10 % Al(V). [6, 22]

The difference in the 28 day hydration sample might be correlated to the change seen in Figure 4.19, where the 28 day sample of Ca/Si = 1.0 also differs from the trends of the higher and lower hydration times, and displays a more ordered structure of C(-A)-S-H. It is possible that a mistake was done during the synthesis of the 28 day hydration time, leading to a higher or lower Al/Si than expected, which might alter the relative amounts of Al in the solids. However, the aqueous concentration of Al in solution follows the same trend as the other Ca/Si series at increasing hydration times, which argues against that. It is also possible that the samples were mislabeled or that the difference in relative amounts of Al species are caused by an error in measurement or in the quantification calculations, although this seems unlikely.

The general increase of Al(VI) with increasing hydration time indicates a higher relative amount of third aluminate hydrate (TAH), which might indicate that TAH is more stable in C-S-H than Al(IV), and that the relative amount of TAH will increase over time. Still, the majority of the Al is found to be Al(IV) tetrahedra bound between two pairing silicate tetrahedra, regardless of hydration time.

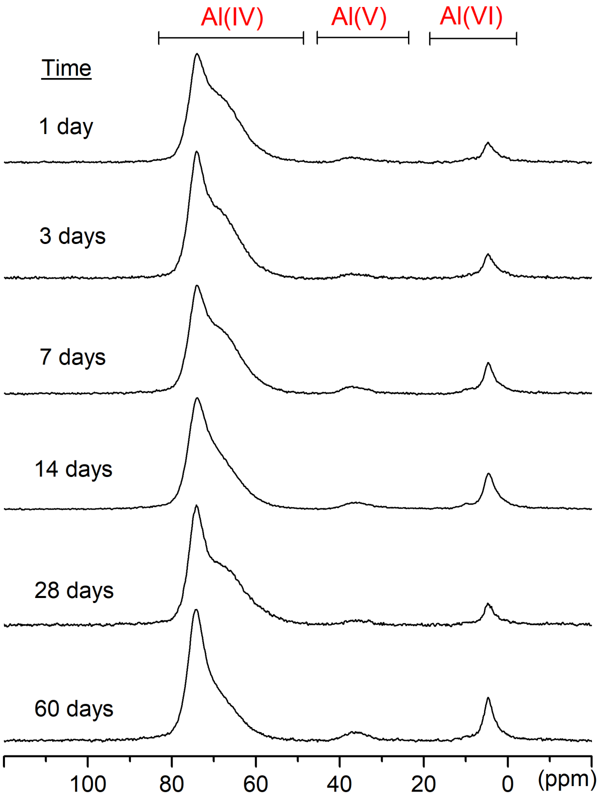

Figure 4.23: ^{27}Al NMR analysis of samples with Ca/Si = 1.0 and target Al/Si = 0.1 with different hydration time.

	Al (IV)	**Al (V)**	**Al (VI)**
1 day	87.1 %	3.7 %	9.2 %
3 days	89.5 %	1.5 %	9.0 %
7 days	85.4 %	3.7 %	10.9 %
14 days	80.4 %	4.4 %	15.2 %
28 days	89.5 %	2.4 %	8.1 %
60 days	81.6 %	4.3 %	14.1 %

Table 4.4: Quantification of aluminium species in Ca/Si = 1.0 and target Al/Si = 0.1, from ^{27}Al NMR analysis.

When it comes to the effect of time on aluminium uptake in C-S-H, several discoveries were made. Firstly, the aqueous concentration of silicon and calcium decreases with increasing hydration time, for target Al/Si = 0.1. Additionally, the aqueous concentration of aluminium decreases rapidly, where the decrease is more apparent in high Ca/Si samples, indicating an affinity of aluminium uptake with increasing Ca/Si.

4.5 Reversibility

Figure 4.24 shows the aqueous concentration of Al in solution of samples with target Al/Si = 0.1 and increasing reversibility time. All the Ca/Si have increasing Al concentrations in solution, although the target Ca/Si of 0.6 has the clearest trend. For target Ca/Si $\geq$ 1.0, the change in concentration of Al is quite stable, and the measured concentrations of Al are overlapping when the measurement error of 10% is taken into account. Increase of Al in solution indicates that some of the Al in the solids has gone into solution, and thus that the Al uptake is reversible in C-S-H for short-term hydration.

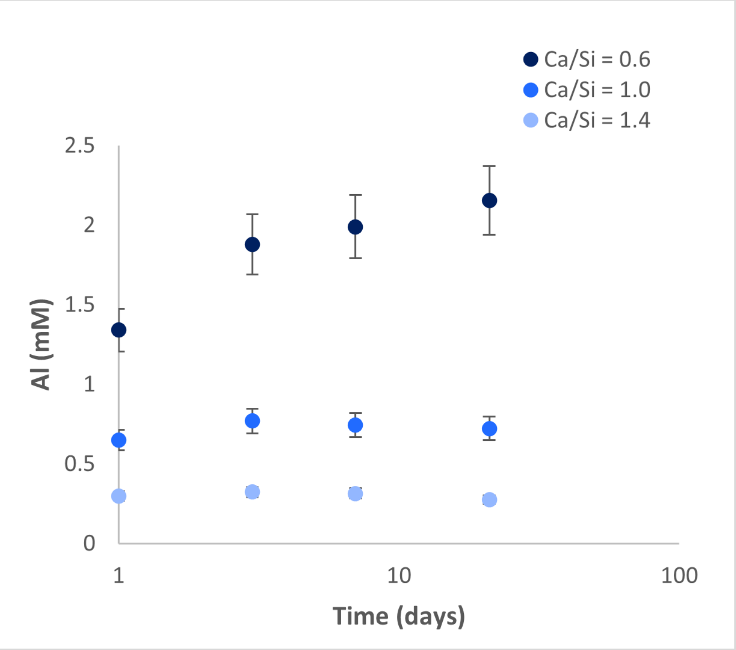

Figure 4.24: Aqueous concentration of aluminium with varying reversibility time and target Ca/Si for target Al/Si = 0.1.

The change of aqueous concentration of Ca in solution with increasing reversibility time is presented in Figure 4.25. For target Ca/Si = 1.0 and 1.4, there is an initial increase of Ca concentration, indicating that some Ca has gone out of the solids and into solution. Then, the aqueous concentration decreases again, as Ca is taken back up into solids. This could be caused by a rearrangement of the C(-A)-S-H during the reversibility period. For target Ca/Si = 0.6, the Ca concentration decreases slightly with time, indicating that Ca is taken up in the solids, while a notable amount of Al is going into solution.

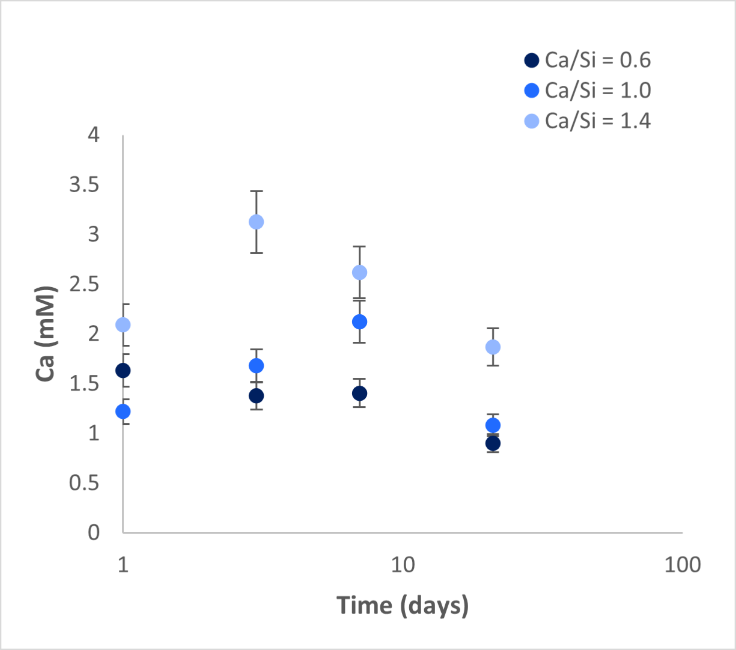

Figure 4.25: Aqueous concentration of calcium with varying reversibility time and target Ca/Si for target Al/Si = 0.1.

Changes in aqueous Si concentration with increasing reversibility time are shown in 4.26 and 4.27. For target Ca/Si = 1.4, the aqueous concentration of Si follows the same trend as Ca, with an initial increase, followed by a decrease. For Ca/Si = 1.0, the concentration of Si decreases slightly initially, before it follows the same trend as for Ca.

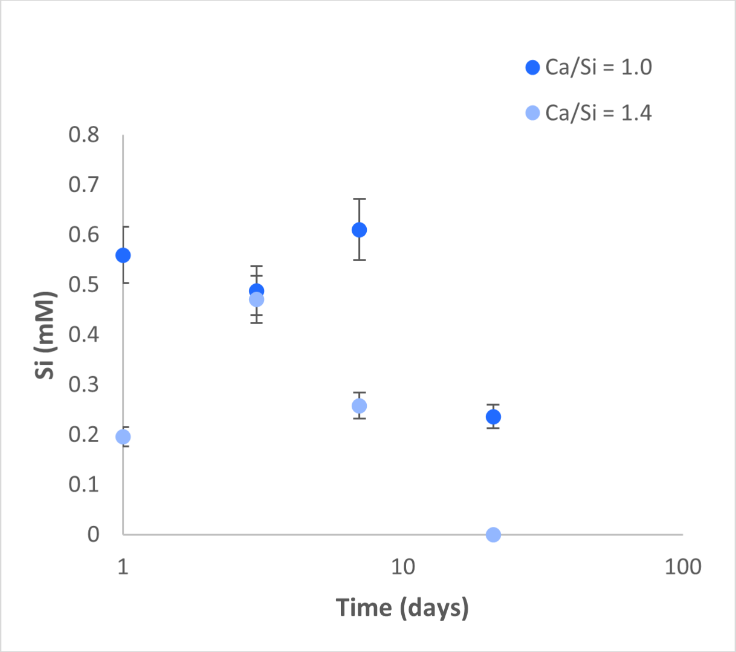

Figure 4.26: Aqueous concentration of silicon with varying reversibility time and target Ca/Si for target Al/Si = 0.1.

Target Ca/Si = 0.6 has an increase of Si in solution with time, indicating that some of the Si in the C(-A)-S-H goes out of the solids and into solution. Though, it is worth noting that the error for each measurement is 10%, which overlaps all of the measured concentrations of Si for Ca/Si = 0.6. Even still, the change in aqueous concentration of Ca and Si correlate for the different Ca/Si series, and together with the release of Al in solution, indicate a rearrangement and possible new formation of C(-A)-S-H as the samples are exposed to solution from C-S-H that is free from Al.

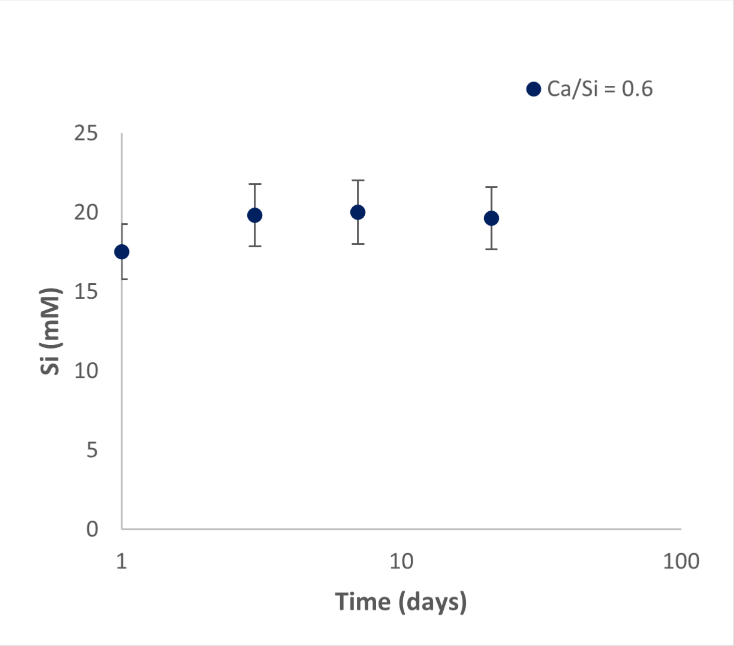

Figure 4.27: Aqueous concentration of silicon with varying reversibility time and target Ca/Si for target Al/Si = 0.1.

Calculated Al/Si in solids are plotted against time in Figure 4.28 and the values are shown in Table 4.5. The calculated Al/Si decreases for all the Ca/Si series, although the trend is most notable in target Ca/Si = 0.6. Thus, the hypothesis of reversibility of Al uptake in C-S-H is further strengthened, and the reversibility is measured to be most prominent with decreasing Ca/Si. This indicates that the Al in the structure of target Ca/Si = 1.4 is more stable than in target Ca/Si = 0.6, which is more reversible.

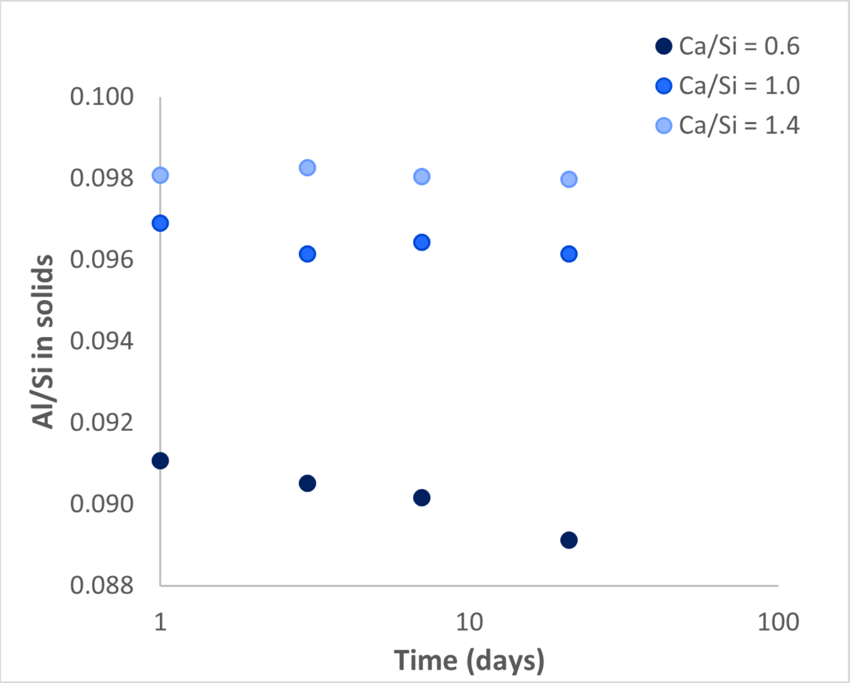

Figure 4.28: Change of Al/Si in solids with increasing reversibility time.

Table 4.5: Table of calculated Ca/Si and Al/Si in solids with target Ca/Si of 0.6, 1.0 and 1.4, for reversibility experiment.

Target Ca/Si	Reversibility time (days)	Ca/Si in solids	Al/Si in solids
0.60	0.25	0.58	0.0914
0.60	1	0.57	0.0911
0.60	3	0.59	0.0905
0.60	7	0.59	0.0902
0.60	21	0.59	0.0891
1.00	0.25	1.00	0.0969
1.00	1	1.00	0.0969
1.00	3	1.00	0.0962
1.00	7	0.99	0.0964
1.00	21	1.00	0.0961
1.40	0.25	1.40	0.0985
1.40	1	1.39	0.0981
1.40	3	1.38	0.0983
1.40	7	1.38	0.0981
1.40	21	1.39	0.0980

Figure 4.29 shows the FT-IR spectra of the target Ca/Si = 0.6 and target Al/Si = 0.1, with varying reversibility times. Interestingly, there are some changes with increasing reversibility time. The peak at 820 cm^{-1}, assigned to Q^1, decreases in intensity with increasing hydration time. Additionally, the main peak at 940

cm^{-1} shifts towards a higher wavenumber with increasing reversibility time. This indicates that the polymerisation increases with increasing reversibility time, which is not expected if there is a decreasing Al/Si in the solids. However, the change in Si and Ca concentration in solution might help explain the change. As both Ca and Si in solution was found to change, at the same time as Al was released into solution, one hypothesis is that the C(-A)-S-H rearranged itself, and as Al went out of solution, Si substituted the bridging sites in the C(-A)-S-H and increased the MCL.

For future projects, it would be interesting to analyse the reversibility samples by ^{27}Al NMR, in order to determine the local environments of Al more clearly, and to shed light on the possible mechanism of the reversibility. Based on the NMR results presented in Section 4.4, a hypothesis could be that the Al is more stable in high Ca/Si because of a higher relative amount of third aluminate hydrate (TAH), while low Ca/Si contains less TAH, and thus releases some of its tetrahedral Al into solution.

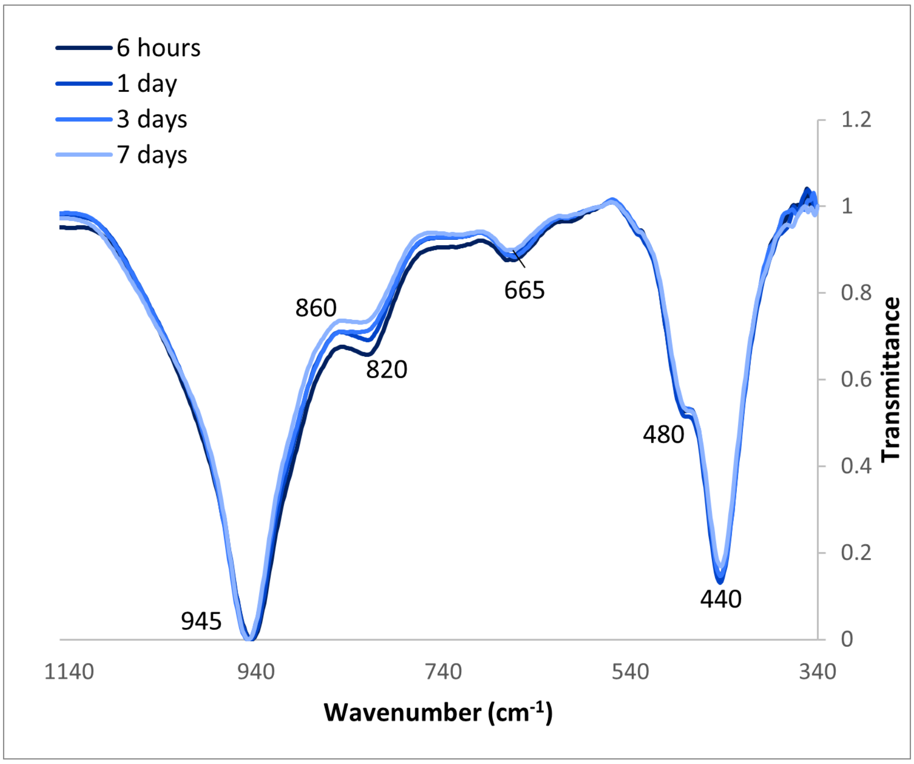

Figure 4.29: FTIR of the of target Ca/Si = 1.0 and target Al/Si = 0.1, for reversibility experiment.

In summary, the aluminium uptake in C-S-H is reversible for low Ca/Si, and seems relatively stable in target Ca/Si ≥ 1.0. The stability in high Ca/Si could be caused by a higher relative amount of TAH, although it cannot be concluded from the data set and analyses done for the reversibility experiment alone.

Conclusion 5

Solid samples of C(-A)-S-H were synthesised, where the calculated Ca/Si in solids were between 0.68 and 1.6 and calculated Al/Si between 0 and 0.09. With increasing Ca/Si, the basal spacing was found to decrease. Similarly, an increase of Al/Si also decreases the basal spacing. Ca/Si $\leq$ 1.0 contain only C(-A)-S-H at target Al/Si $\leq$ 0.05, while Ca/Si $\geq$ 1.2 also contain Portlandite (CH). At target Al/Si = 0.1, all samples with Ca/Si $\geq$ 1.2 contain hemicarbonate and monocarbonate, in addition to C(-A)-S-H and CH.

There is a higher uptake of Na in low Ca/Si, both in the presence and absence of Al. The mean chain length (MCL) of C(-A)-S-H increases with decreasing Ca/Si and increasing Al/Si.

The kinetics of Al uptake increases in high Ca/Si samples. For Ca/Si = 1.0, the local environment for Al changes slightly over time, where a higher ratio of Al(VI) and lower ratio of Al(IV) can be found with increasing hydration time, indicating that third aluminate hydrate (TAH) is more stable in long term hydration.

During the reversibility experiment, Al was found to be more stable in high Ca/Si than in low Ca/Si, presumably due to a higher relative amount of Al(VI) and TAH in high Ca/Si C(-A)-S-H. In target Ca/Si = 0.6, the Al uptake was found to be reversible. This should be considered when using blended cements with a high content of SCMs, as Al could be less stable in the C-S-H phase, compared to in ordinary PC.

Outlook 6

In addition to the experiments and analyses carried out during this project, other methods could have been applied in order to determine the kinetics of aluminium uptake in C-S-H better.

For instance, it would be interesting to look at additional Ca/Si series with ^{29}Si and ^{27}Al NMR. ^{29}Si NMR can be used to understand the changes in polymerisation in the C-S-H, and ^{27}Al NMR can be used to determine the local environment of Al in C-S-H. If the two methods are coupled together on several Ca/Si and Al/Si samples, there could be a greater understanding on the effect of low Al/Si in C-S-H, as previous research primarily has focused on Al/Si $\geq$ 0.1. ^{29}Si and ^{27}Al NMR analyses on reversibility samples could be interesting, to investigate why the reversibility increases with decreasing Ca/Si.

Thermodynamic modelling of the synthesised system could be performed, which could help explain some of the results obtained. For instance, GEM-Selektor could be used for modelling the Saturation Indices (SI) of the solution, based on its composition. The SI could give valuable information on the possibility of precipitation of solids, where a positive SI indicates that the system is oversaturated in regards to that phase, and that it will precipitate. Furthermore, thermodynamic modelling could be used to calculate the expected phases present in all the samples that were synthesised, to compare the results.

The effect of pH can be studied, in order to better understand the effect of pH on Al uptake and reversibility.

Quantitative analysis could be conducted in order to obtain more information on the samples in this project. For instance, the interlayer distances could be calculated, and the composition of C-S-H could be determined.

The samples synthesised in this project have had a maximum hydration time of 90 days. While this is useful for short-term hydration kinetics, the long-term effects cannot be concluded from it. Thus, long-term change in properties could be investigated, to get a broader understanding on long-term hydration and kinetics of C-S-H with Al/Si $\leq$ 0.1.

Thermogravimetric analysis (TGA) was performed on several samples, for references and high Al/Si of target Ca/Si of 0.6, 1.0 and 1.4. In order to get a higher sample size for thermodynamic modelling databases, more samples should be analysed by

TGA. Additionally, Rietveld refinement of samples containing secondary phases could be performed. Rietveld refinement uses X-ray powder diffraction (XRD) samples to calculate the amount of secondary phases present in the solids. Thus, the correct amount of Ca/Si and Al/Si in C-S-H could be calculated, as secondary phases would be taken into account in the mass balance calculations. As the mass balance calculation in this project is based on weigh-in, ion concentration in aqueous solution, and TGA results alone, it is only possible to calculate Al/Si and Ca/Si in solids, and not in C-S-H, for the high Ca/Si with secondary phases.

The solid samples were stored in vacuum desiccators when they were not analysed. However, the samples were exposed to CO_2, and carbonation occured in all samples measured by TGA. In future projects, this carbonation should be avoided, by using better vacuum desiccators during storage, and by minimising unnecessary contact with air.

Bibliography

[1] Miller SA, Myers RJ. Environmental Impacts of Alternative Cement Binders. Environmental Science & Technology. 2020; 54: 677–686.

[2] Barzgar S, Lothenbach B, Tarik M, Giacomo AD, Ludwig C. The effect of sodium hydroxide on Al uptake by calcium silicate hydrates (C-S-H). Journal of Colloid and Interface Science. 2020;572: 246–256.

[3] Thomsen RM. Role of Alkali Calcium Aluminosilicate Glasses in Low Energy Cement. Aalborg University; 2017. PhD dissertation.

[4] L'Hôpital E, Lothenbach B, Saout GL, Kulik D, Scrivener K. Incorporation of aluminium in calcium-silicate-hydrates. Cement and Concrete Research. 2015;75:91–103.

[5] Sakir S, Raman SN, Safiuddin M, Kaish ABMA, Mutalib AA. Utilization of By-Products and Wastes as Supplementary Cementitious Materials in Structural Mortar for Sustainable Construction. Sustainability. 2020; 12: 3888 .

[6] Pardal X, Brunet F, Charpentier T, Pochard I, Nonat A. ^{27}Al and ^{29}Si Solid-State NMR Characterization of Calcium-Aluminosilicate-Hydrate. Inorganic Chemistry. 2012;51:1827–1836.

[7] Lothenbach B, Nonat A. Calcium silicate hydrates: Solid and liquid phase composition. Cement and Concrete Research. 2015;78:57–70.

[8] Monteiro PJM, Miller SA, Horvath A. Towards sustainable concrete. Nature Materials. 2017; 16: 698–699 .

[9] Hewlett PC, Lea FM. Lea's Chemistry of Cement and Concrete. John Wiley & Sons Inc.; 1998.

[10] Gani MSJ. Cement and Concrete. CRC Press; 2017.

[11] Yue Y. Cement Chemistry (II); 2019. Lecture note for Materials Chemistry.

[12] Kajaste R, Hurme M. Cement industry greenhouse gas emissions - management options and abatement cost. Journal of Cleaner Production. 2016;112:4041–4052.

[13] Pourchet S, Regnaud L, Perez JP, Nonat A. Early C_3A hydration in the presence of different kinds of calcium sulfate. Cement and Concrete Research. 2009 nov; 39: 989–996 .

[14] Siddique R, Cachim P. Waste and Supplementary Cementitious Materials in Concrete. Woodhead Publishing; 2018.

[15] Skibsted J, Snellings R. Reactivity of supplementary cementitious materials (SCMs) in cement blends. Cement and Concrete Research. 2019; 124: 1–16.

[16] L'Hôpital E. Aluminium and alkali uptake in calcium silicate hydrates (C-S-H). École Polytechnique Fédérale de Lausanne; 2014. PhD dissertation.

[17] Neville AM. Properties of Concrete. Pearson Education Limited; 2011.

[18] Alizadeh RA. Nanostructure and Engineering Properties of Basic and Modified Calcium-Silicate-Hydrate Systems. University of Ottowa; 2009. PhD dissertation.

[19] Richardson IG. The calcium silicate hydrates. Cement and Concrete Research. 2008; 38 : 137–158 .

[20] Kunther W, Ferreiro S, Skibsted J. Influence of the Ca/Si ratio on the compressive strength of cementitious calcium–silicate–hydrate binders. Journal of Materials Chemistry A. 2017; 5: 17401–17412.

[21] Haas J, Nonat A. From C–S–H to C–A–S–H: Experimental study and thermodynamic modelling. Cement and Concrete Research. 2015; 68: 124–138.

[22] L'Hôpital E, Lothenbach B, Scrivener K, Kulik DA. Alkali uptake in calcium alumina silicate hydrate (C-A-S-H). Cement and Concrete Research. 2016;85:122–136.

[23] Richardson IG, Brough AR, Brydson R, Groves GW, Dobsont CM. Location of Aluminum in Substituted Calcium Silicate Hydrate (C-S-H) Gels as Determined by ^{29}Si and ^{27}Al NMR and EELS. Journal of the American Ceramic Society. 1993; 76 (9): 2285–2288 .

[24] Renaudin G, Russias J, Leroux F, dit Coumes CC, Frizon F. Structural characterization of C–S–H and C–A–S–H samples—Part II: Local environment investigated by spectroscopic analyses. Journal of Solid State Chemistry. 2009; 182 : 3320–3329 .

[25] Yang SY, Yan Y, Lothenbach B, Skibsted J. Incorporation of Sodium and Aluminum in Cementitious Calcium-Alumino-Silicate-Hydrate C-(A)-S-H Phases Studied by ^{23}Na, ^{27}Al and ^{29}Si MAS NMR Spectroscopy. Manuscript submitted for publication. 2021;.

[26] Mohamed AK, Moutzouri P, Berruyer P, Walder BJ, Siramanont J, Harris M, et al. The Atomic-Level Structure of Cementitious Calcium Aluminate Silicate Hydrate. Journal of the American Chemical Society. 2020; 142: 11060–11071.

[27] Barzgar S, Tarik M, Ludwig C, Lothenbach B. The effect of equilibration time on Al uptake in C-S-H. Cement and Concrete Research. 2021; 144: 106438 .

[28] Lodeiro G, Fernández-Jimenez A, Palomo A, Macphee DE. Effect on fresh C-S-H gels of the simultaneous addition of alkali and aluminium. Cement and Concrete Research. 2010; 40: 27–32.

[29] Yan Y, Yang SY, Miron GD, Collings IE, L'Hôpital E, Skibsted J, et al. Effect of alkali hydroxide on calcium silicate hydrate (C-S-H). Manuscript submitted for publication, Cement and Concrete Research. 2021;.

[30] Yu P, Kirkpatrick RJ, Poe B, McMillan PF, Cong X. Structure of Calcium Silicate Hydrate (C-S-H): Near-, Mid-, and Far-Infrared Spectroscopy. Journal of the American Ceramic Society. 1999; 82[3]: 742–748.

[31] Higl J, Hinder D, Rathgeber C, Ramming B, Lindén M. Detailed in situ ATR-FTIR spectroscopy study of the early stages of C-S-H formation during hydration of monoclinic C_3S. Cement and Concrete Research. 2021; 142: 106367 .

[32] Kapeluszna E, Łukasz Kotwica, Rózycka A, Łukasz Gołek. Incorporation of Al in C-A-S-H gels with various Ca/Si and Al/Si ratio: Microstructural and structural characteristics with DTA/TG, XRD, FTIR and TEM analysis. Construction and Building Materials. 2017; 155: 643–653 .

[33] Lothenbach B, Durdzinski PT, de Weerdt K. Thermogravimetric analysis, in Scrivener K, Snellings R, Lothenbach B (Eds.), A Practical Guide to Microstructural Analysis of Cementitious Materials. 1st ed. CRC Press; 2016.

[34] Dong Y, Feng C, Zhao Q, Liang X. Study on the Structure of C-S-H Gels of Slag-Cement Hardened Paste by ^{29}Si, ^{27}Al MAS NMR. Applied Magnetic Resonance. 2019; 50: 1345–1357 .

[35] Andersen MD, Jakobsen HJ, Skibsted J. Incorporation of Aluminum in the Calcium Silicate Hydrate (C-S-H) of Hydrated Portland Cements: A High Field ^{27}Al and ^{29}Si MAS NMR Investigation. Inorganic Chemistry. 2003; 42 (7): 2280–2287 .

[36] Craigie N. Principles of Elemental Chemostratigraphy. Springer International Publishing; 2018.

Synthesis weigh-in A

Chemicals

- Silica fume, SiO_2 - (CAS: 112945-52-5, Sigma-Aldrich)
- Calcium carbonate, $CaCO_3$ - (CAS: 471-34-1, Chemsolute, $\geq$99.5 %)
- Sodium aluminate, $NaAlO_2$ - (CAS: 11138-49-1, Sigma-Aldrich)
- Sodium hydroxide, NaOH - (CAS: 471-34-1, VWR Chemicals, $\geq$99 %)
- Soda lime Drägersorb 400, $Ca(OH)_2 \cdot nNaOH \cdot mH_2O$, for CO_2 capture - (CAS: 1305-62-0, 1310-73-2, 7732-18-5, Dräger)
- Nitric acid, HNO_3 - (CAS: 7697-37-2, Sigma Aldrich, $\geq$65 %)
- Calcium chloride dihydrate, $CaCl_2 \cdot 2\,H_2O$ - (CAS: 10035-04-8, Supelco Merck)
- Ethanol absolute, C_2H_5OH - (CAS: 64-17-5, VWR Chemicals, $\geq$99.8 %)
- Nitric acid, HNO_3 - (CAS: 7697-37-2 ,Suprapur, Merck, $\geq$65 %) - For ICP-OES analysis

Materials

- 20 mL syringes (BD Plastipak)
- Nylone filter membranes, 45 μm pore size (Frisenette)
- Polyethylene containers with lid, 100, 250, and 500 mL
- Polyamide (PA) syringe filters, 45 μm (Phenex)
- Borosilicate glass filtration setup

The masses of CaO and SiO_2 were noted during synthesis and are presented in this Appendix. Samples are categorised by their target Ca/Si and Al/Si molar ratio. ICP-OES analyses on the $NaAlO_2$ solutions were used to calculate the mass of $NaAlO_2$ present in each sample, based on the concentration and the volume added to each sample.

Table A.1: Weigh-in masses of CaO and SiO_2 for the reversibility experiment. Calculated amount of $NaAlO_2$, Ca/Si and Al/Si molar ratio, based on weigh-in.

Target Ca/Si	**Target Al/Si**	**Eq. time in days**	**CaO (g)**	**SiO2 (g)**	**NaAlO2 (g)**
0.6	0	28	2.876	5.128	0
0.8	0	28	3.424	4.581	0
1.0	0	28	3.861	4.142	0
1.2	0	28	4.230	3.777	0
1.4	0	28	4.533	3.469	0
1.6	0	28	4.791	3.211	0
0.6	0.1	28	1.320	2.389	0.321
0.8	0.1	28	1.589	2.125	0.290
1.0	0.1	28	1.809	1.934	0.264
1.2	0.1	28	1.989	1.773	0.242
1.4	0.1	28	2.141	1.638	0.223
1.6	0.1	28	2.272	1.524	0.208

Table A.2: Weigh-in masses of CaO and SiO_2 for the kinetics experiment. Calculated amount of $NaAlO_2$, based on weigh-in and ICP-OES results of the $NaAlO_2$ solutions added to the different samples.

Target Ca/Si	**Target Al/Si**	**CaO (g)**	**SiO2 (g)**	**NaAlO2 (g)**
0.6	0	0.721 +- 0.002	1.284 +- 0.002	0
0.6	0.0003	0.718 +- 0.003	1.281 +- 0.003	5.17E-06
0.6	0.001	0.714 +- 0.001	1.273 +- 0.003	1.90E-05
0.6	0.005	0.689 +- 0.001	1.229 +-0.002	9.20E-05
0.6	0.01	0.662 +- 0.002	1.180 +- 0.002	1.77E-04
0.6	0.05	0.690 +- 0.003	1.230 +- 0.002	0.077
0.6	0.1	0.663 +- 0.004	1.182 +- 0.003	0.158
0.8	0	0.857 +- 0.004	1.147 +- 0.001	0
0.8	0.0003	0.855 +- 0.003	1.144 +- 0.002	4.52E-06
0.8	0.001	0.848 +- 0.001	1.137 +- 0.001	1.51E-05
0.8	0.005	0.824 +- 0.002	1.103 +- 0.002	7.01E-05
0.8	0.01	0.794 +- 0.002	1.063 +- 0.001	1.35E-04
0.8	0.05	0.825 +- 0.001	1.104 +- 0.002	0.069
0.8	0.1	0.796 +- 0.002	1.065 +- 0.003	0.142
1.0	0	0.967 +- 0.003	1.035 +- 0.003	0
1.0	0.0003	0.965 +- 0.001	1.033 +- 0.001	2.013E-06
1.0	0.001	0.960 +- 0.002	1.028 +- 0.001	6.69E-06
1.0	0.005	0.935 +- 0.002	1.000 +- 0.001	3.23E-05
1.0	0.01	0.903 +- 0.002	0.967 +- 0.001	6.26E-05
1.0	0.05	0.936 +- 0.002	1.002 +- 0.001	0.063
1.0	0.1	0.905 +- 0.002	0.970 +- 0.005	0.129
1.2	0	1.057 +- 0.003	0.944 +- 0.002	0
1.2	0.0003	1.056 +- 0.002	0.944 +- 0.001	1.35E-06
1.2	0.001	1.050 +- 0.001	0.938 +- 0.001	3.29E-06
1.2	0.005	1.025 +- 0.002	0.915 +- 0.002	1.36E-05
1.2	0.01	0.994 +- 0.003	0.887 +- 0.001	2.64E-05
1.2	0.05	1.027 +- 0.004	0.916 +- 0.003	0.057
1.2	0.1	0.996 +- 0.004	0.889 +- 0.003	0.119
1.4	0	1.135 +- 0.005	0.868 +-0.003	0
1.4	0.0003	1.132 +- 0.002	0.868 +- 0.001	1.24E-06
1.4	0.001	1.127 +- 0.001	0.862 +- 0.001	3.02E-06
1.4	0.005	1.102 +- 0.002	0.843 +- 0.002	1.25E-05
1.4	0.01	1.071 +- 0.001	0.820 +- 0.001	2.43E-05
1.4	0.05	1.104 +- 0.003	0.842 +- 0.002	0.053
1.4	0.1	1.073 +- 0.003	0.821 +- 0.002	0.049
1.6	0	1.198 +- 0.003	0.804 +- 0.002	0
1.6	0.0003	1.197 +- 0.002	0.803 +- 0.002	1.14E-06
1.6	0.001	1.192 +- 0.001	0.800 +- 0.003	2.80E-06
1.6	0.005	1.167 +- 0.001	0.783 +- 0.001	1.16E-05
1.6	0.01	1.137 +- 0.002	0.763 +- 0.002	2.26E-05

TGA data B

Figure B.1 displays the %CO_2 loss from carbonates, measured by TGA, against Ca/Si, calculated from mass balance. With increasing Ca/Si, there is a general increase of CO_2 present in each sample. This is likely caused by the increased amount of Ca in high Ca/Si. A summary of the TGA results is shown in Table B.1.

The solid samples were stored in three separate desiccators. The desiccators were placed in vacuum, except for when samples were analysed. Although the time of air exposure was kept to a minimum, there was inevitably some exposure to CO_2 for each sample. Furthermore, one desiccator was opened more frequently, as it contained more samples, which further exposed the samples to air. Each desiccator had its own $CaCl_2$ solution and NaOH pellets for capture. The relative humidity was not recorded, and there might have been slight differences between the different desiccators. The samples were not placed in desiccators based on Ca/Si or Al/Si, but rather based on where there was available space. Thus, it is difficult to determine whether some differences in carbonation and water uptake could be caused by the storage of the samples. Even still, when there is a general trend throughout all Ca/Si and/or all Al/Si series, it is considered a real trend, rather than error in measurement or in synthesis and storage.

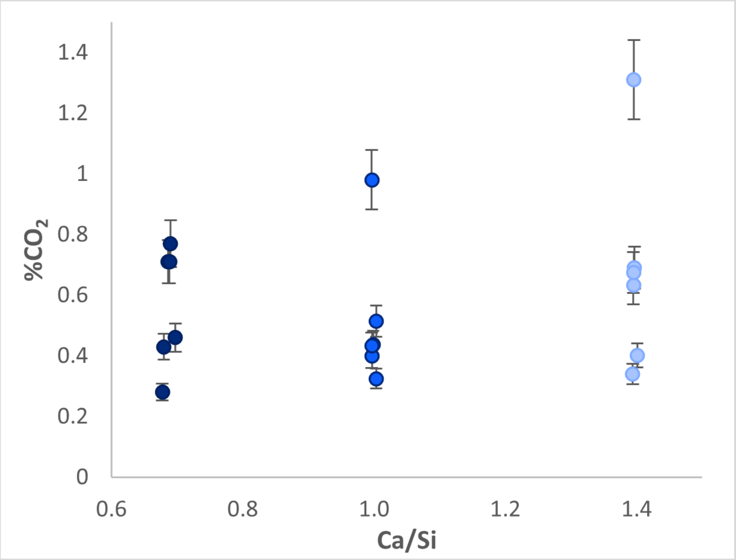

Figure B.1: %CO_2 loss from carbonates, as measured by TGA.

As can be seen from Table B.1, there is a general decrease of H_2O bound in each sample, with increasing Ca/Si. Certain samples do not follow this trend, and show a sudden spike in weight loss due to H_2O. This could be explained by the TGA measurements themselves, as they were not performed successively, but rather over several weeks. The equipment was also used for other experiments, and regularly calibrated, which could further explain some of the discrepancies in the results.

Table B.1: Weight loss of water, CH, and CO2 in reference samples, measured by TGA.

Ca/Si in solids	**Al/Si in solids**	**Hydration time**	**%H_2O loss**	**%CH loss**	**%CO_2 loss**
0.69	0	1	19.77	-	0.71
0.69	0	3	19.95	-	0.77
0.68	0	7	20.22	-	0.43
0.68	0	14	20.28	-	0.28
0.69	0	28	20.15	-	0.71
0.70	0	60	18.19	-	0.46
1.00	0	1	19.03	-	0.51
1.00	0	3	23.20	-	0.33
1.00	0	7	18.24	-	0.44
1.00	0	14	17.72	-	0.40
1.00	0	28	19.54	-	0.98
1.00	0	60	21.84	-	0.43
1.20	0	28	19.98	3.44	0.34
1.40	0	1	19.11	2.85	1.31
1.39	0	3	17.97	3.86	0.63
1.40	0	7	20.93	4.061	0.40
1.39	0	14	19.15	4.86	0.34
1.40	0	28	16.97	4.61	0.69
1.40	0	60	18.97	3.18	0.67
1.60	0	28	16.53	5.26	1.11

Weight loss for phases in target Al/Si = 0.05, as measured by TGA, are presented in Table B.2.

Table B.2: Weight loss of water, CH, and CO_2 in target Al/Si = 0.05, measured by TGA.

Ca/Si in solids	**Al/Si in solids**	**Hydration time**	**%H_2O loss**	**%CH loss**	**%CO_2 loss**
0.71	0.03	1	24.33	-	0.56
0.71	0.03	3	21.48	-	0.77
0.70	0.03	7	22.87	-	1.16
0.69	0.04	14	23.17	-	0.70
0.67	0.04	28	22.59	-	0.37
0.67	0.04	60	20.66	-	0.38
1.00	0.04	1	22.60	-	0.77
1.00	0.04	3	20.50	-	0.62
1.00	0.04	7	24.96	-	1.06
1.00	0.04	14	19.99	-	0.46
1.00	0.04	28	22.79	-	0.65
1.00	0.04	60	22.97	-	0.67
1.19	0.04	28	21.45	1.29	0.76
1.40	0.04	1	18.14	3.13	0.80
1.39	0.04	3	18.56	2.82	0.98
1.40	0.04	7	20.25	2.36	1.16
1.40	0.04	14	19.06	2.65	0.83
1.40	0.05	28	19.41	2.92	0.77
1.40	0.05	60	18.90	2.71	1.03

Weight loss for phases in target Al/Si = 0.1, as measured by TGA, are presented in Table B.3.

Table B.3: Weight loss of water, CH, and CO2 in target Al/Si = 0.1, measured by TGA.

Ca/Si in solids	**Al/Si in solids**	**Hydration time**	**%H_2O loss**	**%CH loss**	**%CO_2 loss**
0.68	0.07	1	20.86	-	0.65
0.72	0.10	3	20.72	-	0.80
0.73	0.10	7	20.73	-	0.39
0.69	0.10	14	22.24	-	0.63
0.68	0.09	28	22.90	-	0.43
0.66	0.09	60	21.54	-	0.45
1.00	0.08	1	23.23	-	0.96
1.00	0.09	3	20.90	-	0.64
1.00	0.09	7	20.39	-	0.74
1.00	0.09	14	22.04	-	0.54
1.00	0.09	28	20.62	-	0.52
1.00	0.09	60	20.36	-	0.30
1.20	0.08	28	22.11	1.75	0.41
1.39	0.08	1	20.32	2.29	1.68
1.39	0.09	3	17.02	4.30	0.58
1.40	0.09	7	17.11	4.40	0.55
1.40	0.09	14	17.15	4.52	0.57
1.39	0.09	28	18.88	2.56	0.82
1.40	0.09	60	18.30	3.73	0.68

Mass balance of samples C

The calculated mass balance of the samples for the kinetics experiment is presented in Table C.1 and for the reversibility experiment in Table C.2. The mass balance is based on the initial weigh-in, where the amount of moles of each element is calculated. Then, the moles of elements present in solution are calculated from the ICP-OES results. The mass balance of each element is obtained by subtracting moles of element in solution from moles of element from the weigh-in.

Table C.1: Aqueous concentration of Al, Ca, Si, and Na in solution, measured by ICP-OES.

Ca/Si target	**Al/Si target**	**Hydration time**	**Ca/Si in solids**	**Al/Si in solids**
0.6	0	1	0.69	0
0.6	0	3	0.69	0
0.6	0	7	0.68	0
0.6	0	14	0.68	0
0.6	0	28	0.69	0
0.6	0	90	0.70	0
0.6	0.0003	1	0.69	1.88E-04
0.6	0.0003	3	0.70	1.43E-04
0.6	0.0003	7	0.69	1.82E-04
0.6	0.0003	14	0.68	1.65E-04
0.6	0.0003	28	0.66	2.29E-04
0.6	0.0003	90	0.70	2.14E-04
0.6	0.001	1	0.69	6.72E-04
0.6	0.001	3	0.68	6.75E-04
0.6	0.001	7	0.67	6.89E-04
0.6	0.001	14	0.68	6.83E-04
0.6	0.001	28	0.68	7.87E-04
0.6	0.001	90	0.68	7.58E-04
0.6	0.005	1	0.67	3.47E-03
0.6	0.005	3	0.68	3.55E-03
0.6	0.005	7	0.67	3.59E-03
0.6	0.005	14	0.68	3.59E-03
0.6	0.005	28	0.67	3.90E-03

Ca/Si target	**Al/Si target**	**Hydration time**	**Ca/Si in solids**	**Al/Si in solids**
0.6	0.005	90	0.69	3.96E-03
0.6	0.01	1	0.68	6.71E-03
0.6	0.01	3	0.67	6.97E-03
0.6	0.01	7	0.68	7.04E-03
0.6	0.01	14	0.67	7.02E-03
0.6	0.01	28	0.67	7.65E-03
0.6	0.01	90	0.69	7.76E-03
0.6	0.05	1	0.71	2.55E-02
0.6	0.05	3	0.71	3.21E-02
0.6	0.05	7	0.70	3.45E-02
0.6	0.05	14	0.69	4.46E-02
0.6	0.05	28	0.67	4.36E-02
0.6	0.05	60	0.67	4.30E-02
0.6	0.1	1	0.68	6.78E-02
0.6	0.1	3	0.72	1.01E-01
0.6	0.1	7	0.73	1.03E-01
0.6	0.1	14	0.69	9.69E-02
0.6	0.1	28	0.68	9.49E-02
0.6	0.1	60	0.66	8.87E-02
0.8	0	1	0.81	0
0.8	0	3	0.81	0
0.8	0	7	0.81	0
0.8	0	14	0.81	0
0.8	0	28	0.81	0
0.8	0	90	0.80	0
0.8	0.0003	1	0.81	2.04E-04
0.8	0.0003	3	0.81	2.19E-04
0.8	0.0003	7	0.81	2.19E-04
0.8	0.0003	14	0.81	2.17E-04
0.8	0.0003	28	0.81	2.22E-04
0.8	0.0003	90	0.81	2.19E-04
0.8	0.001	1	0.81	7.12E-04
0.8	0.001	3	0.81	7.29E-04
0.8	0.001	7	0.81	7.34E-04
0.8	0.001	14	0.81	7.32E-04
0.8	0.001	28	0.81	7.48E-04
0.8	0.001	90	0.81	7.60E-04
0.8	0.005	1	0.81	3.42E-03
0.8	0.005	3	0.81	3.45E-03
0.8	0.005	7	0.81	3.45E-03

Ca/Si target	**Al/Si target**	**Hydration time**	**Ca/Si in solids**	**Al/Si in solids**
0.8	0.005	14	0.81	3.51E-03
0.8	0.005	28	0.81	3.55E-03
0.8	0.005	90	0.81	3.65E-03
0.8	0.01	1	0.81	6.68E-03
0.8	0.01	3	0.81	6.80E-03
0.8	0.01	7	0.81	6.86E-03
0.8	0.01	14	0.81	7.32E-03
0.8	0.01	28	0.81	7.01E-03
0.8	0.01	90	0.80	7.27E-03
0.8	0.05	1	0.81	3.60E-02
0.8	0.05	3	0.81	3.70E-02
0.8	0.05	7	0.81	3.78E-02
0.8	0.05	14	0.81	4.24E-02
0.8	0.05	28	0.81	4.24E-02
0.8	0.05	60	0.81	4.23E-02
0.8	0.1	1	0.81	7.37E-02
0.8	0.1	3	0.82	8.47E-02
0.8	0.1	7	0.81	8.59E-02
0.8	0.1	14	0.81	8.68E-02
0.8	0.1	28	0.81	8.83E-02
0.8	0.1	60	0.81	8.67E-02
1.0	0	1	1.00	0
1.0	0	3	1.00	0
1.0	0	7	1.00	0
1.0	0	14	1.00	0
1.0	0	28	1.00	0
1.0	0	90	1.00	0
1.0	0.0003	1	1.00	9.85E-05
1.0	0.0003	3	1.00	1.05E-04
1.0	0.0003	7	1.00	1.05E-04
1.0	0.0003	14	1.00	1.02E-04
1.0	0.0003	30	1.00	7.62E-05
1.0	0.0003	90	1.00	1.05E-04
1.0	0.001	1	1.00	1.70E-04
1.0	0.001	3	1.00	1.76E-04
1.0	0.001	7	1.00	1.79E-04
1.0	0.001	14	1.00	1.76E-04
1.0	0.001	30	1.00	1.86E-04
1.0	0.001	90	1.00	1.82E-04
1.0	0.005	1	1.00	1.83E-03

Ca/Si target	**Al/Si target**	**Hydration time**	**Ca/Si in solids**	**Al/Si in solids**
1.0	0.005	3	1.00	1.87E-03
1.0	0.005	7	1.00	1.88E-03
1.0	0.005	14	1.00	1.89E-03
1.0	0.005	30	1.00	1.91E-03
1.0	0.005	90	1.00	1.90E-03
1.0	0.01	1	1.00	3.18E-03
1.0	0.01	3	1.00	3.51E-03
1.0	0.01	7	1.00	3.70E-03
1.0	0.01	14	1.00	3.71E-03
1.0	0.01	30	1.00	3.75E-03
1.0	0.01	90	1.00	3.82E-03
1.0	0.05	1	1.00	3.72E-02
1.0	0.05	3	1.00	3.85E-02
1.0	0.05	7	1.00	3.92E-02
1.0	0.05	14	1.00	4.35E-02
1.0	0.05	28	1.00	4.42E-02
1.0	0.05	60	1.00	4.43E-02
1.0	0.1	1	1.00	8.21E-02
1.0	0.1	3	1.00	8.77E-02
1.0	0.1	7	1.00	8.92E-02
1.0	0.1	14	1.00	8.99E-02
1.0	0.1	28	1.00	9.01E-02
1.0	0.1	60	1.00	9.01E-02
1.2	0	1	1.20	0
1.2	0	3	1.19	0
1.2	0	7	1.19	0
1.2	0	14	1.19	0
1.2	0	28	1.20	0
1.2	0	90	1.19	0
1.2	0.0003	1	1.20	7.22E-05
1.2	0.0003	3	1.20	7.91E-05
1.2	0.0003	7	1.19	7.92E-05
1.2	0.0003	14	1.19	7.21E-05
1.2	0.0003	28	1.19	7.56E-05
1.2	0.0003	90	1.19	7.57E-05
1.2	0.001	1	1.19	1.89E-04
1.2	0.001	3	1.19	2.00E-04
1.2	0.001	7	1.19	2.00E-04
1.2	0.001	14	1.20	1.96E-04
1.2	0.001	28	1.20	2.00E-04

Ca/Si target	**Al/Si target**	**Hydration time**	**Ca/Si in solids**	**Al/Si in solids**
1.2	0.001	90	1.19	2.00E-04
1.2	0.005	1	1.20	8.61E-04
1.2	0.005	3	1.20	8.75E-04
1.2	0.005	7	1.20	8.78E-04
1.2	0.005	14	1.20	8.75E-04
1.2	0.005	28	1.20	8.79E-04
1.2	0.005	90	1.19	8.76E-04
1.2	0.01	1	1.20	1.66E-03
1.2	0.01	3	1.20	1.75E-03
1.2	0.01	7	1.20	1.75E-03
1.2	0.01	14	1.20	1.76E-03
1.2	0.01	28	1.20	1.76E-03
1.2	0.01	90	1.20	1.77E-03
1.2	0.05	1	1.19	3.83E-02
1.2	0.05	3	1.20	3.96E-02
1.2	0.05	7	1.20	4.12E-02
1.2	0.05	14	1.19	4.40E-02
1.2	0.05	28	1.19	4.48E-02
1.2	0.05	60	1.21	4.52E-02
1.2	0.1	1	1.19	7.53E-02
1.2	0.1	3	1.19	8.28E-02
1.2	0.1	7	1.19	8.19E-02
1.2	0.1	14	1.20	8.23E-02
1.2	0.1	28	1.20	8.45E-02
1.2	0.1	60	1.20	8.53E-02
1.4	0	1	1.40	0
1.4	0	3	1.39	0
1.4	0	7	1.40	0
1.4	0	14	1.39	0
1.4	0	28	1.40	0
1.4	0	90	1.40	0
1.4	0.0003	1	1.40	7.10E-05
1.4	0.0003	3	1.39	7.85E-05
1.4	0.0003	7	1.39	7.48E-05
1.4	0.0003	14	1.39	7.46E-05
1.4	0.0003	28	1.39	7.46E-05
1.4	0.0003	90	1.39	7.84E-05
1.4	0.001	1	1.39	1.91E-04
1.4	0.001	3	1.40	1.99E-04
1.4	0.001	7	1.39	1.99E-04

Ca/Si target	**Al/Si target**	**Hydration time**	**Ca/Si in solids**	**Al/Si in solids**
1.4	0.001	14	1.40	1.99E-04
1.4	0.001	28	1.40	2.00E-04
1.4	0.001	90	1.39	1.99E-04
1.4	0.005	1	1.39	8.60E-04
1.4	0.005	3	1.39	8.65E-04
1.4	0.005	7	1.39	8.71E-04
1.4	0.005	14	1.40	8.78E-04
1.4	0.005	28	1.40	8.77E-04
1.4	0.005	90	1.40	8.78E-04
1.4	0.01	1	1.39	1.67E-03
1.4	0.01	3	1.40	1.73E-03
1.4	0.01	7	1.39	1.75E-03
1.4	0.01	14	1.40	1.76E-03
1.4	0.01	28	1.40	1.77E-03
1.4	0.01	90	1.39	1.76E-03
1.4	0.05	1	1.40	3.79E-02
1.4	0.05	3	1.39	3.93E-02
1.4	0.05	7	1.40	4.06E-02
1.4	0.05	14	1.40	4.46E-02
1.4	0.05	28	1.40	4.60E-02
1.4	0.05	60	1.40	4.53E-02
1.4	0.1	1	1.39	7.87E-02
1.4	0.1	3	1.39	9.13E-02
1.4	0.1	7	1.40	9.20E-02
1.4	0.1	14	1.40	9.23E-02
1.4	0.1	28	1.39	9.30E-02
1.4	0.1	60	1.40	9.37E-02
1.6	0	1	1.60	0
1.6	0	3	1.59	0
1.6	0	7	1.59	0
1.6	0	14	1.59	0
1.6	0	28	1.60	0
1.6	0	90	1.59	0
1.6	0.0003	1	1.60	6.57E-05
1.6	0.0003	3	1.59	5.74E-05
1.6	0.0003	7	1.59	7.39E-05
1.6	0.0003	14	1.59	6.98E-05
1.6	0.0003	28	1.59	6.98E-05
1.6	0.0003	90	1.59	7.38E-05
1.6	0.001	1	1.59	1.90E-04

Ca/Si target	**Al/Si target**	**Hydration time**	**Ca/Si in solids**	**Al/Si in solids**
1.6	0.001	3	1.59	1.93E-04
1.6	0.001	7	1.60	1.94E-04
1.6	0.001	14	1.60	1.94E-04
1.6	0.001	28	1.59	1.94E-04
1.6	0.001	90	1.59	1.93E-04
1.6	0.005	1	1.59	8.20E-04
1.6	0.005	3	1.59	8.62E-04
1.6	0.005	7	1.59	8.65E-04
1.6	0.005	14	1.59	8.71E-04
1.6	0.005	28	1.60	8.71E-04
1.6	0.005	90	1.59	8.71E-04
1.6	0.01	1	1.59	1.44E-03
1.6	0.01	3	1.59	1.66E-03
1.6	0.01	7	1.58	1.72E-03
1.6	0.01	14	1.60	1.74E-03
1.6	0.01	28	1.59	1.74E-03
1.6	0.01	90	1.59	1.75E-03

Table C.2: Mass balance calculations of reversibility samples. Ca/Si and Al/Si in solids are calculated.

Ca/Si target	Al/Si target	Reversibility time (days)	Ca/Si in solids	Al/Si in solids
0.60	0.1	0.25	0.58	9.14E-02
0.60	0.1	1	0.57	9.11E-02
0.60	0.1	3	0.59	9.05E-02
0.60	0.1	7	0.59	9.02E-02
0.60	0.1	21	0.59	8.91E-02
1.00	0.1	0.25	0.79	9.52E-02
0.80	0.1	1	0.79	9.51E-02
0.80	0.1	3	0.78	9.42E-02
0.80	0.1	7	0.78	9.40E-02
0.80	0.1	21	0.79	9.38E-02
1.00	0.1	0.25	1.00	9.69E-02
1.00	0.1	1	1.00	9.69E-02
1.00	0.1	3	1.00	9.62E-02
1.00	0.1	7	0.99	9.64E-02
1.00	0.1	21	1.00	9.61E-02
1.20	0.1	0.25	1.20	9.82E-02
1.20	0.1	1	1.20	9.83E-02
1.20	0.1	3	1.18	9.78E-02
1.20	0.1	7	1.19	9.79E-02
1.20	0.1	21	1.20	9.82E-02
1.40	0.1	0.25	1.40	9.85E-02
1.40	0.1	1	1.39	9.81E-02
1.40	0.1	3	1.38	9.83E-02
1.40	0.1	7	1.38	9.81E-02
1.40	0.1	21	1.39	9.80E-02
1.60	0.1	0.25	1.60	9.72E-02
1.60	0.1	1	1.59	9.84E-02
1.60	0.1	3	1.59	9.86E-02
1.60	0.1	7	1.59	9.91E-02
1.60	0.1	21	1.59	9.85E-02

Concentration of elements D

The aqueous concentration of Al, Ca, Si, and Na in solution was measured by ICP-OES, and is displayed in Table D.1. ICP-OES uses plasma and a spectrometer to measure the concentration. The solution that is analysed is nebulised into a spray chamber, where it is led into an argon plasma. An alternar magnetic field is induced and accelerates the electrons into a circular trajectory. The argon atoms and electrons collide, leading to ionisation, which leads to a stable plasma with an extremely high temperature, typically between 6000-7000 K. The electrons reach an excited state due to the thermic energy they absorb. As they drop back to ground level energy, they release energy in the form of photons. Each element has its own characteristic emission spectrum that can be recorded, and the intensity of the wavelength determines the concentration, as the system is calibrated with samples of known concentration beforehand. [36]

Table D.1: Aqueous concentration of Al, Ca, Si, and Na in solution, measured by ICP-OES.

Target Ca/Si	**Target Al/Si**	**Eq. time in days**	**[Al] mmol/L**	**[Ca] mmol/L**	**[Si] mmol/L**	**[Na] mmol/L**
0.6	0.0	1	0.002	0.01	29.24	409.4
0.6	0.0003	1	0.018	0.02	29.74	430.2
0.6	0.001	1	0.047	0.02	31.33	420.8
0.6	0.005	1	0.188	0.03	24.92	440.9
0.6	0.01	1	0.411	0.03	25.42	431.7
0.6	0.05	1	5.550	0.02	34.14	538.8
0.6	0.1	1	8.434	0.02	26.72	502.3
0.8	0.0	1	0.002	0.04	1.74	428.5
0.8	0.0003	1	0.009	0.04	1.69	430.5
0.8	0.001	1	0.020	0.03	2.31	437.3
0.8	0.005	1	0.088	0.04	1.87	431.9
0.8	0.01	1	0.201	0.04	2.02	430.4
0.8	0.05	1	2.088	0.05	2.40	550.9
0.8	0.1	1	5.013	0.04	3.23	513.1
1.0	0.0	1	0.002	0.41	0.66	449.8
1.0	0.0003	1	0.004	0.39	0.20	449.8
1.0	0.001	1	0.005	0.39	0.20	458.6

Target Ca/Si	**Target Al/Si**	**Eq. time in days**	**[Al] mmol/L**	**[Ca] mmol/L**	**[Si] mmol/L**	**[Na] mmol/L**
1.0	0.005	1	0.021	0.40	0.20	451.6
1.0	0.01	1	0.128	0.28	0.26	446.1
1.0	0.05	1	1.684	0.36	0.51	607.8
1.0	0.1	1	2.835	0.32	0.41	554.5
1.2	0.0	1	0.002	0.76	0.19	461.0
1.2	0.0003	1	0.002	0.71	0.10	469.3
1.2	0.001	1	0.004	0.76	0.10	470.3
1.2	0.005	1	0.005	0.75	0.10	467.1
1.2	0.01	1	0.023	0.98	0.12	384.2
1.2	0.05	1	1.233	1.16	0.20	620.7
1.2	0.1	1	2.421	1.29	0.18	605.1
1.4	0.0	1	0.002	0.70	0.48	465.7
1.4	0.0003	1	0.002	0.76	0.10	472.7
1.4	0.001	1	0.003	0.74	0.10	470.9
1.4	0.005	1	0.005	0.74	0.10	467.2
1.4	0.01	1	0.043	1.00	0.12	383.8
1.4	0.05	1	1.305	1.25	0.19	638.6
1.4	0.1	1	2.862	1.05	0.19	596.7
1.6	0.0	1	0.002	0.66	0.55	430.6
1.6	0.0003	1	0.003	0.80	0.09	473.3
1.6	0.001	1	0.003	0.82	0.09	471.1
1.6	0.005	1	0.010	0.80	0.09	474.4
1.6	0.01	1	0.049	0.78	0.10	470.3
0.6	0.0	3	0.002	0.00	30.01	375.2
0.6	0.0003	3	0.028	0.03	32.53	441.7
0.6	0.001	3	0.044	0.03	27.64	439.3
0.6	0.005	3	0.173	0.03	25.19	441.4
0.6	0.01	3	0.350	0.02	23.72	436.4
0.6	0.05	3	4.300	0.03	36.25	552.8
0.6	0.1	3	3.158	0.04	36.95	422.3
0.8	0.0	3	0.003	0.05	1.80	439.3
0.8	0.0003	3	0.005	0.04	1.67	427.9
0.8	0.001	3	0.016	0.03	1.91	434.4
0.8	0.005	3	0.084	0.03	2.28	440.5
0.8	0.01	3	0.181	0.03	2.25	433.4
0.8	0.05	3	1.915	0.04	3.49	567.5
0.8	0.1	3	2.899	0.06	4.28	436.7
1.0	0.0	3	0.003	0.39	0.26	477.1
1.0	0.0003	3	0.002	0.40	0.20	453.8
1.0	0.001	3	0.004	0.38	0.20	456.5

Target Ca/Si	**Target Al/Si**	**Eq. time in days**	**[Al] mmol/L**	**[Ca] mmol/L**	**[Si] mmol/L**	**[Na] mmol/L**
1.0	0.005	3	0.013	0.37	0.21	453.2
1.0	0.01	3	0.069	0.29	0.25	445.2
1.0	0.05	3	1.428	0.31	0.48	598.8
1.0	0.1	3	1.750	0.30	0.30	471.7
1.2	0.0	3	0.003	0.93	0.11	498.5
1.2	0.0003	3	0.001	0.71	0.10	463.4
1.2	0.001	3	0.002	0.71	0.11	466.6
1.2	0.005	3	0.003	0.72	0.11	481.7
1.2	0.01	3	0.019	0.98	0.10	385.8
1.2	0.05	3	1.050	1.14	0.20	636.4
1.2	0.1	3	1.142	0.65	0.09	501.3
1.4	0.0	3	0.003	0.98	0.10	515.3
1.4	0.0003	3	0.001	0.75	0.10	475.8
1.4	0.001	3	0.002	0.76	0.10	469.1
1.4	0.005	3	0.004	0.76	0.10	475.3
1.4	0.01	3	0.017	1.03	0.09	386.9
1.4	0.05	3	1.079	1.26	0.20	648.5
1.4	0.1	3	0.911	0.79	0.07	507.0
1.6	0.0	3	0.003	1.00	0.10	517.4
1.6	0.0003	3	0.004	0.82	0.09	480.6
1.6	0.001	3	0.002	0.84	0.09	463.4
1.6	0.005	3	0.004	0.81	0.09	476.3
1.6	0.01	3	0.018	0.83	0.09	476.7
0.6	0.0	7	0.003	0.06	28.36	444.8
0.6	0.0003	7	0.019	0.02	29.81	440.7
0.6	0.001	7	0.039	0.03	25.21	437.2
0.6	0.005	7	0.162	0.02	24.73	438.7
0.6	0.01	7	0.347	0.02	25.48	437.3
0.6	0.05	7	3.774	0.02	33.51	548.8
0.6	0.1	7	2.783	0.05	36.38	425.6
0.8	0.0	7	0.003	0.03	2.97	457.9
0.8	0.0003	7	0.005	0.04	1.52	431.5
0.8	0.001	7	0.016	0.03	2.38	443.0
0.8	0.005	7	0.081	0.03	2.18	442.0
0.8	0.01	7	0.166	0.04	1.80	437.3
0.8	0.05	7	1.734	0.06	2.43	560.3
0.8	0.1	7	2.550	0.06	2.85	452.6
1.0	0.0	7	0.002	0.44	0.21	484.7
1.0	0.0003	7	0.002	0.55	0.28	467.4
1.0	0.001	7	0.003	0.56	0.29	468.8

Target Ca/Si	**Target Al/Si**	**Eq. time in days**	**[Al] mmol/L**	**[Ca] mmol/L**	**[Si] mmol/L**	**[Na] mmol/L**
1.0	0.005	7	0.011	0.49	0.31	463.8
1.0	0.01	7	0.034	0.44	0.33	458.4
1.0	0.05	7	1.303	0.28	0.53	598.0
1.0	0.1	7	1.564	0.27	0.33	484.4
1.2	0.0	7	0.002	0.88	0.11	505.8
1.2	0.0003	7	0.001	0.75	0.10	462.5
1.2	0.001	7	0.002	0.72	0.10	456.5
1.2	0.005	7	0.002	0.73	0.10	464.0
1.2	0.01	7	0.005	1.01	0.10	388.1
1.2	0.05	7	0.745	1.21	0.19	644.5
1.2	0.1	7	1.266	0.79	0.10	506.9
1.4	0.0	7	0.002	0.94	0.10	502.9
1.4	0.0003	7	0.002	0.76	0.10	472.4
1.4	0.001	7	0.002	0.76	0.10	472.7
1.4	0.005	7	0.003	0.77	0.10	469.4
1.4	0.01	7	0.005	1.10	0.09	390.3
1.4	0.05	7	0.863	1.26	0.19	648.9
1.4	0.1	7	0.849	1.14	0.07	1051.2
1.6	0.0	7	0.003	0.97	0.10	518.4
1.6	0.0003	7	0.002	0.80	0.09	465.9
1.6	0.001	7	0.002	0.83	0.09	472.5
1.6	0.005	7	0.004	0.84	0.09	479.0
1.6	0.01	7	0.009	0.83	0.09	475.5
0.6	0.0	14	0.003	0.01	27.16	441.3
0.6	0.0003	14	0.023	0.03	26.63	438.3
0.6	0.001	14	0.041	0.04	26.61	434.6
0.6	0.005	14	0.166	0.03	25.97	441.6
0.6	0.01	14	0.338	0.03	23.19	433.2
0.6	0.05	14	1.629	0.04	30.41	448.6
0.6	0.1	14	3.061	0.02	29.68	444.6
0.8	0.0	14	0.004	0.06	1.85	449.2
0.8	0.0003	14	0.006	0.02	2.75	441.4
0.8	0.001	14	0.016	0.03	1.93	441.3
0.8	0.005	14	0.069	0.03	1.92	440.8
0.8	0.01	14	0.077	0.04	1.87	437.2
0.8	0.05	14	0.787	0.08	1.79	464.5
0.8	0.1	14	2.399	0.04	2.82	442.1
1.0	0.0	14	0.004	0.45	0.21	479.4
1.0	0.0003	14	0.003	0.40	0.19	459.4
1.0	0.001	14	0.004	0.40	0.19	445.9

Target Ca/Si	**Target Al/Si**	**Eq. time in days**	**[Al] mmol/L**	**[Ca] mmol/L**	**[Si] mmol/L**	**[Na] mmol/L**
1.0	0.005	14	0.011	0.34	0.22	452.6
1.0	0.01	14	0.031	0.30	0.24	431.3
1.0	0.05	14	0.485	0.26	0.40	502.7
1.0	0.1	14	1.407	0.22	0.36	492.2
1.2	0.0	14	0.004	0.89	0.11	500.9
1.2	0.0003	14	0.002	0.73	0.10	482.8
1.2	0.001	14	0.002	0.73	0.10	477.1
1.2	0.005	14	0.003	0.71	0.10	477.3
1.2	0.01	14	0.004	1.02	0.10	384.6
1.2	0.05	14	0.254	0.78	0.12	524.7
1.2	0.1	14	1.232	0.54	0.14	517.8
1.4	0.0	14	0.004	0.93	0.10	505.8
1.4	0.0003	14	0.002	0.76	0.10	485.2
1.4	0.001	14	0.002	0.77	0.10	476.3
1.4	0.005	14	0.002	0.77	0.09	478.3
1.4	0.01	14	0.004	1.10	0.09	387.0
1.4	0.05	14	0.248	1.10	0.08	540.9
1.4	0.1	14	0.809	0.88	0.09	531.7
1.6	0.0	14	0.004	0.96	0.10	507.7
1.6	0.0003	14	0.002	0.84	0.09	483.6
1.6	0.001	14	0.002	0.85	0.09	480.0
1.6	0.005	14	0.003	0.85	0.09	487.5
1.6	0.01	14	0.006	0.85	0.09	493.1
0.6	0.0	28	0.004	0.04	30.86	444.3
0.6	0.0003	28	0.008	0.04	22.62	433.9
0.6	0.001	28	0.021	0.04	27.64	437.5
0.6	0.005	28	0.096	0.04	23.60	443.8
0.6	0.01	28	0.197	0.04	21.27	429.4
0.6	0.05	28	1.558	0.01	24.13	472.3
0.6	0.1	28	3.126	0.12	26.31	435.2
0.8	0.0	28	0.003	0.07	1.83	450.7
0.8	0.0003	28	0.005	0.08	1.97	437.5
0.8	0.001	28	0.012	0.07	1.90	437.9
0.8	0.005	28	0.063	0.08	1.95	440.4
0.8	0.01	28	0.138	0.07	2.11	437.1
0.8	0.05	28	0.768	0.05	1.90	472.4
0.8	0.1	28	2.012	0.16	1.64	465.9
1.0	0.0	28	0.003	0.59	0.17	483.5
1.0	0.0003	30	0.008	0.47	0.31	457.6
1.0	0.001	30	0.002	0.52	0.28	458.6

Target Ca/Si	**Target Al/Si**	**Eq. time in days**	**[Al] mmol/L**	**[Ca] mmol/L**	**[Si] mmol/L**	**[Na] mmol/L**
1.0	0.005	30	0.007	0.49	0.31	453.4
1.0	0.01	30	0.026	0.40	0.35	448.7
1.0	0.05	28	0.382	0.23	0.41	510.8
1.0	0.1	28	1.346	0.30	0.42	495.0
1.2	0.0	28	0.004	0.92	0.11	503.1
1.2	0.0003	28	0.002	0.97	0.18	483.6
1.2	0.001	28	0.002	1.08	0.17	484.8
1.2	0.005	28	0.002	0.98	0.17	482.1
1.2	0.01	28	0.005	1.03	0.11	384.9
1.2	0.05	28	0.145	1.03	0.09	543.8
1.2	0.1	28	0.939	0.92	0.10	529.9
1.4	0.0	28	0.004	0.99	0.10	507.5
1.4	0.0003	28	0.002	0.99	0.17	496.0
1.4	0.001	28	0.002	1.02	0.17	491.7
1.4	0.005	28	0.002	1.01	0.17	486.9
1.4	0.01	28	0.003	0.98	0.17	486.5
1.4	0.05	28	0.004	1.11	0.10	388.4
1.4	0.1	28	0.165	1.08	0.08	541.7
1.4	0.1	28	0.666	1.23	0.08	530.8
1.6	0.0	28	0.004	0.99	0.10	512.9
1.6	0.0003	28	0.002	0.83	0.08	480.0
1.6	0.001	28	0.002	0.82	0.09	479.2
1.6	0.005	28	0.003	0.83	0.09	486.0
1.6	0.01	28	0.005	0.84	0.09	488.1
0.6	0.0	90	0.007	0.00	32.94	400.5
0.6	0.0003	90	0.013	0.01	32.69	405.5
0.6	0.001	90	0.026	0.01	27.62	393.8
0.6	0.005	90	0.106	0.01	29.76	401.7
0.6	0.01	90	0.220	0.01	26.84	397.1
0.6	0.05	60	1.741	0.01	24.93	403.3
0.6	0.1	60	3.924	0.03	20.93	369.9
0.8	0.0	90	0.002	0.06	1.47	479.8
0.8	0.0003	90	0.005	0.10	1.66	472.7
0.8	0.001	90	0.010	0.11	1.52	474.8
0.8	0.005	90	0.039	0.10	1.64	485.1
0.8	0.01	90	0.083	0.11	1.65	477.5
0.8	0.05	60	0.795	0.04	1.95	416.9
0.8	0.1	60	2.349	0.05	2.38	374.5
1.0	0.0	90	0.002	0.45	0.23	509.0
1.0	0.0003	90	0.002	0.49	0.22	498.7

Target Ca/Si	**Target Al/Si**	**Eq. time in days**	**[Al] mmol/L**	**[Ca] mmol/L**	**[Si] mmol/L**	**[Na] mmol/L**
1.0	0.001	90	0.002	0.58	0.19	496.0
1.0	0.005	90	0.009	0.49	0.24	494.7
1.0	0.01	90	0.013	0.46	0.24	498.1
1.0	0.05	60	0.343	0.20	0.40	439.5
1.0	0.1	60	1.281	0.14	0.45	363.4
1.2	0.0	90	0.001	0.96	0.10	519.3
1.2	0.0003	90	0.002	1.01	0.10	531.8
1.2	0.001	90	0.002	1.10	0.09	525.9
1.2	0.005	90	0.002	1.07	0.10	532.5
1.2	0.01	90	0.002	1.04	0.10	386.9
1.2	0.05	60	0.100	0.93	0.06	463.8
1.2	0.1	60	0.776	0.86	0.06	428.9
1.4	0.0	90	0.002	1.07	0.09	531.7
1.4	0.0003	90	0.001	1.06	0.10	542.5
1.4	0.001	90	0.002	1.07	0.09	531.6
1.4	0.005	90	0.002	1.09	0.09	541.8
1.4	0.01	90	0.002	1.12	0.09	389.0
1.4	0.05	60	0.123	0.97	0.06	472.6
1.4	0.1	60	0.549	1.11	0.04	441.4
1.6	0.0	90	0.002	1.14	0.10	538.2
1.6	0.0003	90	0.002	1.18	0.09	538.4
1.6	0.001	90	0.002	1.23	0.09	551.0
1.6	0.005	90	0.003	1.16	0.09	542.3
1.6	0.01	90	0.004	1.23	0.08	557.9